

Ecological Frontiers

Geospatial technology-based MCDA and machine learning algorithms: an ensemble and inter-evaluating frameworks for conceptualizing groundwater potential

--Manuscript Draft--

Manuscript Number:	ECOFRO-D-25-00323
Article Type:	Full Length Article
Keywords:	AHP; AU-ROC; Fishnet; Groundwater potential; Machine learning; Multicollinearity
Corresponding Author:	Kesyton Oyamenda Ozegin, PhD Ambrose Alli University Ekpmoma, --- elect One --- NIGERIA
First Author:	Kesyton Oyamenda Ozegin, PhD
Order of Authors:	Kesyton Oyamenda Ozegin, PhD Soliu Ademola Mudashiru, MSc Jude Steven Ejepu, PhD
Manuscript Region of Origin:	Africa
Abstract:	<p>Humanity's usage of water cannot be halted, as water is a necessary resource for existence and is highly valued in a variety of quotidian usages and initiatives. Hence, reliable identification of groundwater potential locations in diverse geographical areas (from low to high) is critical for ensuring its management and stability. This study aimed to predict and define groundwater potential (GWP) zones by combining machine learning (ML) models, such as random forest (RF), support vector machine (SVM), adaptive boosting (AdaBoost), and eXtreme gradient boost (XGB), with analytical hierarchy process (AHP)—multi-criteria decision analysis (MCDA) that integrates anthropological (normalized difference vegetation index), hydrogeological (geology and lineament density), hydrological (rainfall distribution and proximity to surface water bodies), and topographical factors (slope, aspect, drainage density, and topographic wetness index) as groundwater-influencing parameters. Prognostication competencies of these factors were established through the application of multicollinearity (MC) evaluation. The AHP approach was used to weight and scale these influencing variables and determine their impact on groundwater prospects. Given the constrained amount of data available, 'CreateFishnet_management' requires training the ML models with 100% borehole data. Every model's reliability was quantified using the area under the receiver-operating characteristic (AU-ROC) curve. The four (4) machine learning algorithms and AHP model divided the GWP zone into four distinct groups: high, moderate, low, and very low. The RF, AdaBoost, SVM, XGB, and AHP models show that the beneficial GWP zones encompass 41.59%, 36.42%, 45.93%, 25.30%, and 14.03% of the research region, respectively. The model dependability using measured AU-ROC curve metrics indicates that the RF model has the greatest rate of success (78.00%), preceding the AdaBoost (77.00%), SVM (73.00%), XGB (71.00%), and AHP (50.00%) models. Consequently, this multi-approach gives valuable perspectives to promote long-term groundwater governance, directing choices on the advancement of the availability of groundwater.</p>
Opposed Reviewers:	

I, Ozegin, K.O., on behalf of my co-authors, wish to submit a manuscript titled '**Geospatial technology-based MCDA and machine learning algorithms: an ensemble and inter-evaluating frameworks for conceptualizing groundwater potential**' for review.

This study aimed to predict and define groundwater potential (GWP) zones by combining machine learning (ML) models, such as random forest (RF), support vector machine (SVM), adaptive boosting (AdaBoost), and eXtreme gradient boost (XGB), with analytical hierarchy process (AHP)—multi-criteria decision analysis (MCDA) that integrates anthropological, hydrogeological, hydrological, and topographical factors as groundwater-influencing parameters. Prognostication competencies of these factors were established through the application of multicollinearity (MC) evaluation. The AHP approach was used to weight and scale these influencing variables and determine their impact on groundwater prospects. Given the constrained amount of data available, 'CreateFishnet_management' requires training the ML models with 100% borehole data. Every model's reliability was quantified using performance statistics and area under the receiver-operating characteristic (AU-ROC) curve. The four (4) machine learning algorithms and AHP model divided the GWP zone into four distinct groups: high, moderate, low, and very low. The RF, AdaBoost, SVM, XGB, and AHP models show that the beneficial GWP zone covers 41.59%, 36.42%, 45.93%, 25.30%, and 14.03% of the research region, respectively. The model dependability using measured AU-ROC curve metrics indicates that the RF model has the greatest rate of success (78.00%), preceding the AdaBoost (77.00%), SVM (73.00%), XGB (71.00%), and AHP (50.00%) models. Consequently, this multi-approach gives valuable perspectives to promote long-term groundwater governance, directing choices on the advancement of the availability of groundwater.

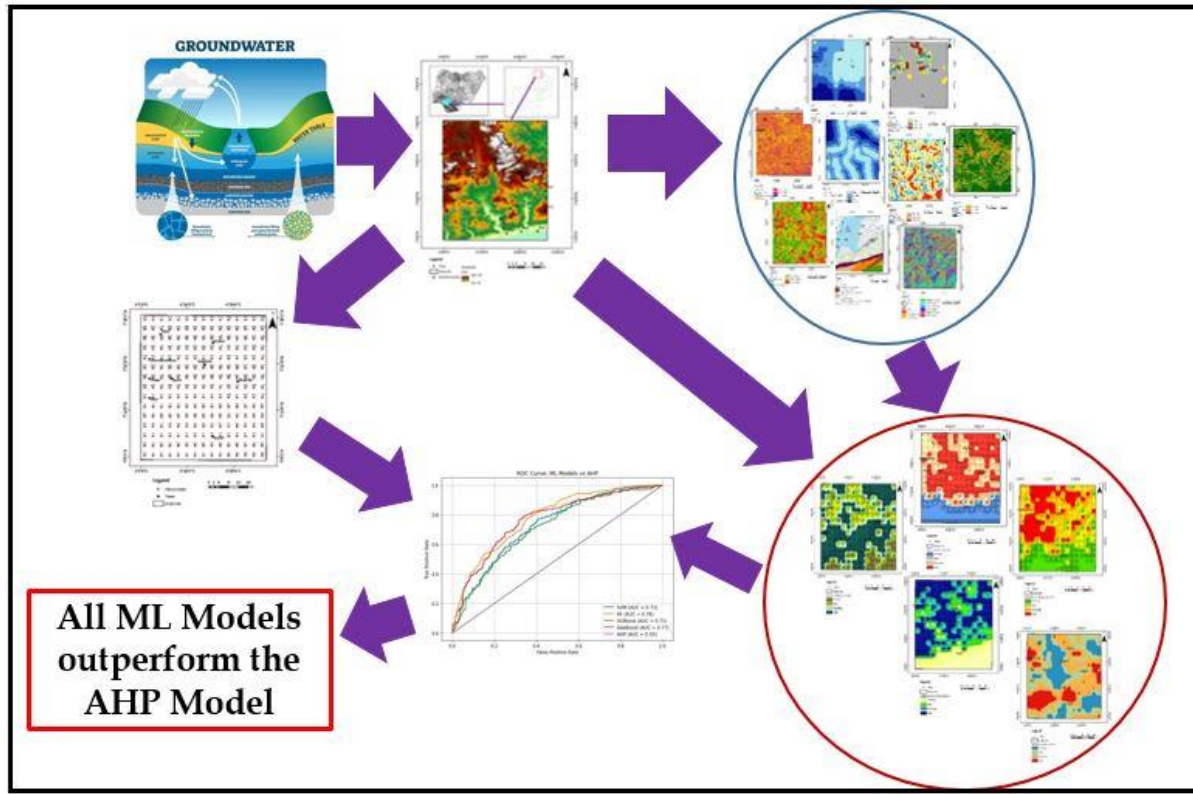
Kesyton Oyamenda Ozegin ^{a*}, Soliu Ademola Mudashiru^b, Jude Steven Ejepu^c

^aDepartment of Physics, Ambrose Alli University Ekpoma, Edo State, Nigeria

^bDepartment of Applied Geophysics, Federal University of Technology, Akure, Nigeria

^cDepartment of Geology, Federal University of Technology, Minna, Niger State, Nigeria

*Corresponding author's e-mail: ozeginkess@yahoo.com



Geospatial technology-based MCDA and machine learning algorithms: an ensemble and inter-evaluating frameworks for conceptualizing groundwater potential

Kesyton Oyamenda Ozegin^{a*}, Soliu Ademola Mudashiru^b, Jude Steven Ejepu^c

^aDepartment of Physics, Ambrose Alli University Ekpoma, Edo State, Nigeria

^bDepartment of Applied Geophysics, Federal University of Technology, Akure, Nigeria

^cDepartment of Geology, Federal University of Technology, Minna, Niger State, Nigeria

*Corresponding author's e-mail: ozeginkess@yahoo.com

Abstract

Humanity's usage of water cannot be halted, as water is a necessary resource for existence and is highly valued in a variety of quotidian usages and initiatives. Hence, reliable identification of groundwater potential locations in diverse geographical areas (from low to high) is critical for ensuring its management and stability. This study aimed to predict and define groundwater potential (GWP) zones by combining machine learning (ML) models, such as random forest (RF), support vector machine (SVM), adaptive boosting (AdaBoost), and eXtreme gradient boost (XGB), with analytical hierarchy process (AHP)—multi-criteria decision analysis (MCDA) that integrates anthropological (normalized difference vegetation index), hydrogeological (geology and lineament density), hydrological (rainfall distribution and proximity to surface water bodies), and topographical factors (slope, aspect, drainage density, and topographic wetness index) as groundwater-influencing parameters. Prognostication competencies of these factors were established through the application of multicollinearity (MC) evaluation. The AHP approach was used to weight and scale these influencing variables and determine their impact on groundwater prospects. Given the constrained amount of data available, 'CreateFishnet_management' requires training the ML models with 100% borehole data. Every model's reliability was quantified using the area under the receiver-operating characteristic (AU-ROC) curve. The four (4) machine learning algorithms and AHP model divided the GWP zone into four distinct groups: high, moderate, low, and very low. The RF, AdaBoost, SVM, XGB, and AHP models show that the beneficial GWP zones encompass 41.59%, 36.42%, 45.93%, 25.30%, and 14.03% of the research region, respectively. The model dependability using measured AU-ROC curve metrics indicates that the RF model has the greatest rate of success (78.00%), preceding the AdaBoost (77.00%), SVM (73.00%), XGB (71.00%), and AHP (50.00%) models. Consequently, this multi-approach gives valuable perspectives to promote long-term groundwater governance, directing choices on the advancement of the availability of groundwater.

Keywords: AHP; AU-ROC; Fishnet; Groundwater potential; Machine learning; Multicollinearity

1 **Geospatial technology-based MCDA and machine learning algorithms: an ensemble and inter-**
2 **evaluating frameworks for conceptualizing groundwater potential**

3 Kesyon Oyamenda Ozegin^{a*}, Soliu Ademola Mudashiru^b, Jude Steven Ejepu^c

5 ^aDepartment of Physics, Ambrose Alli University Ekpoma, Edo State, Nigeria

6 ^bDepartment of Applied Geophysics, Federal University of Technology, Akure, Nigeria

7 ^cDepartment of Geology, Federal University of Technology, Minna, Niger State, Nigeria

9 *Corresponding author's e-mail: ozeginkess@yahoo.com

10 **Abstract**

11 Humanity's usage of water cannot be halted, as water is a necessary resource for existence and is highly valued in
12 a variety of quotidian usages and initiatives. Hence, reliable identification of groundwater potential locations in
13 diverse geographical areas (from low to high) is critical for ensuring its management and stability. This study
14 aimed to predict and define groundwater potential (GWP) zones by combining machine learning (ML) models,
15 such as random forest (RF), support vector machine (SVM), adaptive boosting (AdaBoost), and eXtreme gradient
16 boost (XGB), with analytical hierarchy process (AHP)—multi-criteria decision analysis (MCDA) that integrates
17 anthropological (normalized difference vegetation index), hydrogeological (geology and lineament density),
18 hydrological (rainfall distribution and proximity to surface water bodies), and topographical factors (slope, aspect,
19 drainage density, and topographic wetness index) as groundwater-influencing parameters. Prognostication
20 competencies of these factors were established through the application of multicollinearity (MC) evaluation. The
21 AHP approach was used to weight and scale these influencing variables and determine their impact on
22 groundwater prospects. Given the constrained amount of data available, 'CreateFishnet_management' requires
23 training the ML models with 100% borehole data. Every model's reliability was quantified using the area under
24 the receiver-operating characteristic (AU-ROC) curve. The four (4) machine learning algorithms and AHP model
25 divided the GWP zone into four distinct groups: high, moderate, low, and very low. The RF, AdaBoost, SVM,
26 XGB, and AHP models show that the beneficial GWP zones encompass 41.59%, 36.42%, 45.93%, 25.30%, and
27 14.03% of the research region, respectively. The model dependability using measured AU-ROC curve metrics
28 indicates that the RF model has the greatest rate of success (78.00%), preceding the AdaBoost (77.00%), SVM
29 (73.00%), XGB (71.00%), and AHP (50.00%) models. Consequently, this multi-approach gives valuable
30 perspectives to promote long-term groundwater governance, directing choices on the advancement of the
31 availability of groundwater.

32 **Keywords:** AHP; AU-ROC; Fishnet; Groundwater potential; Machine learning; Multicollinearity

33
34
35

36

37

38

39

40

41

42

43

44

45

46

47

48

49

50

51

52 **1. Introduction**

53 The crucial significance of water to humanity is widely acknowledged—water resources are required for the
54 continued existence of individuals, organisms, and ecosystems (e.g., Ozegin et al., 2023; Kaya et al., 2023; Ozegin
55 et al., 2024a; Chatterjee et al., 2024; UNWWDR, 2025). Population growth and rising economies have created an
56 increased need for access to water. Currently, over forty percent of mankind is facing a shortage of water, and if
57 this trend continues, over 6.3 billion people (globally) will be affected by various levels of water-related problems
58 by 2030 (Opoku et al., 2024). In the three preceding centuries, approximately eighty-five percent of the world's
59 wetlands have been desiccated, while the other 15% of wetlands have deteriorated in quality (UN DESA, 2023;
60 Opoku et al., 2024). The Sustainable Development Goals (SDGs) are built on the sustained existence as well as
61 management of fundamental water supplies, with the goal of providing "access to clean water and sanitation (SDG
62 6), zero hunger (Goal 2), and good health and well-being (Goal 3) through sustainable management of terrestrial
63 ecosystems and their services (SDG 15) and mitigating the effects of climate change (SDG 13)" (United Nations,
64 2015). Thereby strengthening sustainable water, food, and energy nexuses and fostering perspectives for a reliable
65 water future. Given the ever-increasing need for water and a dearth of freshwater resources, a shortage of water
66 presents serious problems, including inadequate access to water, farming impacts, ecological damage, and social
67 and economic inequality. Furthermore, changes in the climate exacerbate water scarcity concerns by altering
68 trends in precipitation, lengthening the degree, severity, and incidence of droughts.

69 According to Scanlon et al. (2023), over two billion people worldwide rely on groundwater (GW) for their water
70 requirements on a daily basis. Considering the rising worldwide shortages of water, the immense potential benefits
71 of groundwater can hardly be discounted. GW, considered an integral part of the hydrologic process, is essential
72 for the survival of several ecosystems, both aquatic and terrestrial. Present-day extraction of groundwater accounts
73 for roughly 26% of all freshwater removal worldwide (Van der Gun, 2012). The frequency of removal of
74 groundwater globally has at least increased threefold and continues to rise at a pace of approximately 0.5-1.0%
75 annually. Specifically, global extractions of freshwater rose 14% between 2000 and 2021—representing a mean yearly
76 increase of 0.7%. As stated by the most contemporary worldwide estimates (from 2021), agriculture accounts for 72%
77 of freshwater extractions, preceded by industry (15%) and home (or municipal) consumption (13%) (UNWWDR, 2025).
78 Sector-driven extractions of freshwater vary greatly depending on the economic growth of a nation. Higher-income
79 nations utilize greater amounts of water for industry, while low-income countries use ninety percent or greater for
80 agricultural irrigation. As climate change makes water supply increasingly unpredictable, groundwater serves as a key
81 reserve during seasons of scarcity, increasing the significance of aquifers for preserving water. GW is a critical
82 worldwide resource that stores the most freshwater, aside from glaciers (WWQA, 2021). The overall quantity of water
83 on the earth is projected to be 1386 trillion litres, with oceans (salt water) accounting for 97% of the water (Senanayake
84 et al., 2016). Of the remaining 3% of freshwater, two-thirds is frozen in ice caps. Less than 1% (0.67) of the world's
85 water is viable freshwater, and groundwater constitutes about 97 percent of total usable freshwater (UNWWDR, 2022;
86 Ozegin et al., 2024a).

87 The accessibility of water is an ongoing issue for billions of people throughout the globe! Water-scarce urban
88 populations are estimated to be 1.7–2.4 billion globally by 2050, from 930 million as of 2016 (United Nations,
89 2023). The lack of water affects the African continent both physically and economically. Physically, it is mostly
90 caused by the depletion of resources as a result of climate change and human activity. While economic constraint
91 comes when water is inaccessible due to inadequate capacity or organizational failings requiring a concerted effort,
92 which is Africa's major issue. Nigeria possesses an abundance of water assets, but the government hasn't leveraged
93 them to their fullest ability to give its citizenry a consistent and adequate supply of drinkable water at an affordable
94 price (e.g., Kolawole, 2015; Ozegin et al., 2023). With a projected population of over 215 million, Nigeria is
95 among the six largest populated nations around the world (UN DESA, 2022; Ozegin and Ilugbo, 2024), making
96 the issue of water scarcity extremely onerous. With only 61% of Nigerians having access to safe water for
97 consumption and an estimated 71 million individuals still requiring improved water services, the country's water
98 industry is beset by serious problems (World Bank Group, 2017; Adewumi et al., 2020; Ozegin et al., 2024b). A
99 large portion of the study area is underpinned with impermeable or nearly impervious materials. Improper
100 borehole placement and considerable borehole failure probabilities are frequently caused by adverse
101 hydrogeological settings and a lack of information about aquifers. Furthermore, accessing water is especially
102 difficult in locations where precipitation is low or uneven, as well as in areas where the consequences of climate
103 change tend to be more severe. According to Ozegin et al. (2023), the bulk of the aquifer networks within the
104 research area are composed of crystalline and basaltic sediments that are distinguished by secondary porosity,

lineaments, and fragmented rocks. The penetrability exhibited by these unconfined aquifers is comparatively higher, and their ability to hold water is diminutive. Based on hydrogeological settings, approximately 76% of the research region's land area comprises hard rocks possibly exhibiting low groundwater potential, with the remaining 24% consisting of sedimentary deposits that have possibly significant potential for groundwater (Ozegin et al., 2023). Sedimentary rock is only found in the southern section of the research area (Ozegin et al., 2023).

Considering the intrinsic variability of hard-rock aquifers, identifying optimal spots for groundwater (also known as groundwater potential or groundwater potential (GWP) zones) is difficult and necessitates an extensive knowledge of all variables that control the accessibility of groundwater in the study area. Groundwater supply and movement are influenced by topography, hydrology, ecology, geology, and the atmosphere (e.g., Oh et al. 2011; Golkarian et al. 2018; Arshad et al., 2020; Ilugbo et al., 2023a; Reza et al., 2023). Groundwater researchers are increasingly employing these parameters to establish groundwater potential (e.g., Al-Shabeb et al., 2018; Ozegin et al., 2024a, b). To ensure the continued viability of water management strategies and to effectively evaluate the availability of groundwater in the study area, a thorough understanding of the features and dynamics of aquifers—geological structures that hold and distribute water—is required using machine learning (ML) and geoinformatics-based methods for the geohydrological assessment of groundwater-enriching sites.

In broad terms, there are two main approaches for assessing groundwater potential in any area: standard techniques and advanced methods—expert decision frameworks and machine learning (see Ozdemir, 2011; Agarwal et al., 2013; Naghibi et al., 2016; Guru et al., 2017; Abrams et al., 2018; Mohammadi-Behzad et al., 2019; Arefin, 2020). The standard approach is based on traditional field surveys, which are laborious and costly. Expert decision frameworks include the analytical hierarchy process (AHP), weighted overlay method, evidential belief function (EBF), fuzzy AHP, and stepwise weight assessment ratio analysis (SWARA) (e.g., Arefin, 2020; Abrar et al., 2021; Fajemilo and Ozegin, 2025), whereas ML algorithms (MLAs) include random forest (RF), artificial neural network (ANN), K-nearest neighbour (KNN), gradient boosting (GB), and so on. These advanced approaches provide more accurate and dependable results than conventional approaches for assessing GW potential (Lee et al., 2012; Das, 2019; Rana et al., 2025). ML models commonly rely on enormous amounts of data, which are either not readily accessible or inadequate in multiple practical realities of hydrologic situations. This difficulty has sparked interest in expert decision frameworks. The application of geospatial-based MCDA and hybrid learning models has significantly improved GWP mapping reliability. Arguably the most common approach for modelling an area with potential for groundwater is to combine a variety of ML algorithms and AHP approaches with geospatial (GIS and remote sensing (RS)) technology (Hasanuzzaman et al., 2022; Dey et al., 2023; Rana et al., 2025). Acknowledging the drawbacks of conventional techniques, this study proposes an innovative amalgamation of machine learning (ML) models, including random forest (RF), support vector machine (SVM), adaptive boosting (AdaBoost), and eXtreme gradient boost (XGB), with analytical hierarchy process (AHP) approaches within a GIS structure. By integrating these cutting-edge methods with varied datasets, this study provides a quint-perspective strategy for groundwater potential modelling that improves reliability and usability in the research area.

ML algorithms are a recently developed technique that has produced fascinating outcomes (Vafadar et al., 2023; Fajemilo and Ozegin, 2025). The models are entirely based on computer technologies and are designed to address tough problems involving exponential and intricate datasets. The fundamental advantage of algorithms is that they deal directly with unprocessed data, which substantially decreases experts' influence. Several research studies (e.g., Lee et al., 2012; Naghibi and Pourghasemi, 2015; Rahmati et al., 2016; Sahoo et al., 2017; Golkarian et al., 2018; Lee et al., 2018; Chen et al., 2019; Sameen et al., 2019; Avand et al., 2020; Maskooni et al., 2020; Patidar et al., 2021; Karimi-Rizvandi et al., 2021; Pham et al., 2021; Hasanuzzaman et al., 2022; Vafadar et al., 2023; Shandu and Atif, 2023; Khan and Jhamnani, 2023; Sharma et al., 2024; Rana et al., 2025) have used ML algorithms to map groundwater potential zones, including random forest (RF), eXtreme gradient boost (XGB), logistic regression (LR), classification and regression tree (CART), support vector machine (SVM), adaptive boosting (AdaBoost), genetic algorithm (GA), and K-neighbour (KN). These researchers created reliable maps with high levels of accuracy and yielded convincing outcomes. The random forest (RF), support vector machine (SVM), adaptive boosting (AdaBoost), and eXtreme gradient boost (XGB) were chosen for the study because they have been reported to be more efficient than other MLAs such as genetic algorithm, boosted regression tree (BRT), artificial neural network model, classification and regression tree, and LR (Naghibi et al., 2017; Moghaddam et al., 2020; Patidar et al., 2021; Vafadar et al., 2023). While these machine learning algorithms are capable of handling various predictive features and facilitating fitting interactions between indicators (e.g., Olden et al. 2008; Khan and Jhamnani, 2023), they are additionally susceptible to overfitting data, which makes fishnet (FN) analysis crucial. The prediction power of the four chosen ML algorithms is additionally contrasted to guarantee the dependability of the resulting GWP zones map.

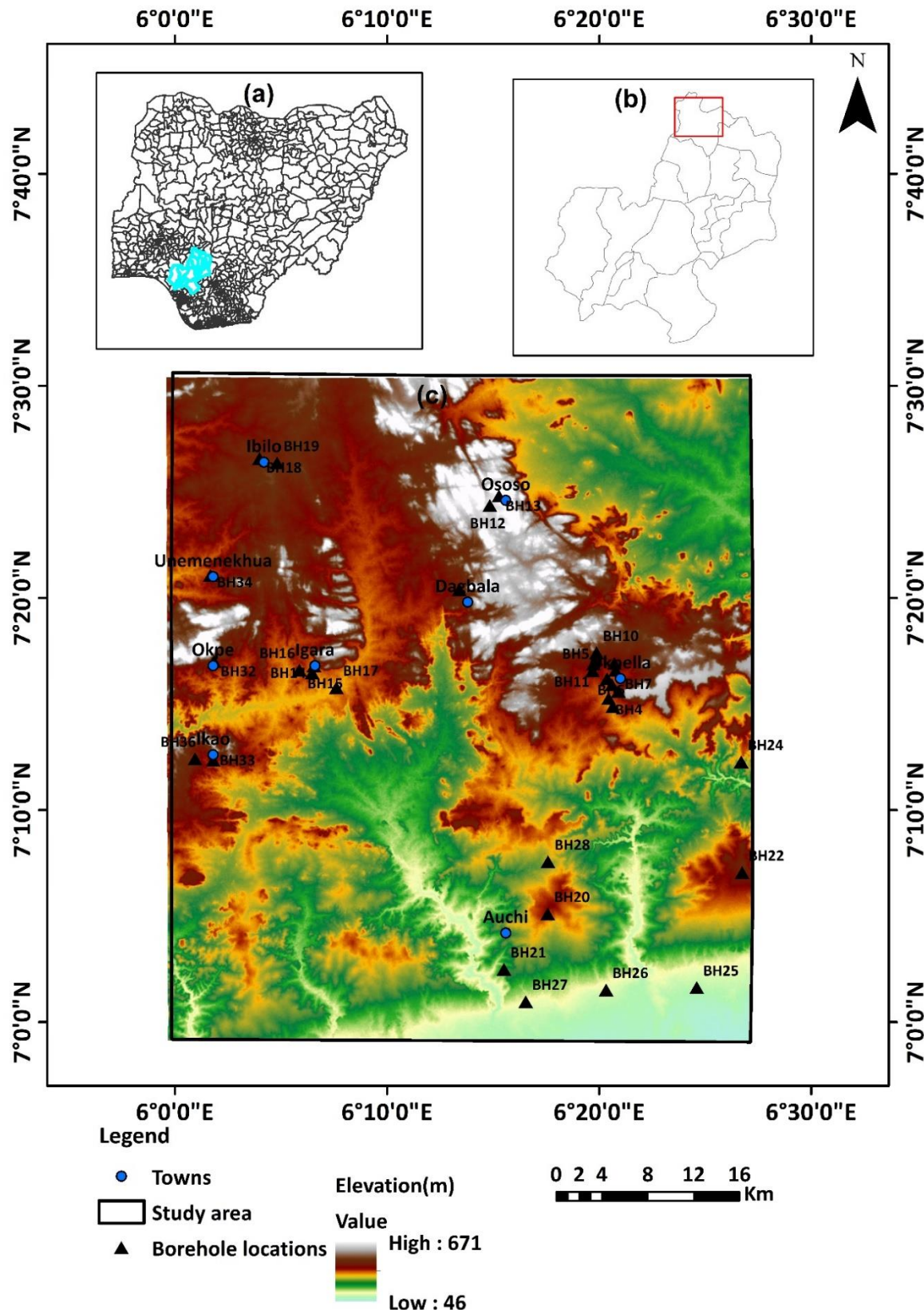
160 Remote sensing technologies are developing rapidly, and a significant amount of RS materials are freely available globe-
161 wide. These can be used to identify global driving features and effectively calculate GW's future potential. RS data and
162 GIS technology play a pivotal part in locating and mapping possible groundwater sites. For evaluating GWP zones, this
163 study espoused the expert judgment system known as the analytical hierarchical process (AHP). Spatial challenges such
164 as exploring groundwater present a multiple-attribute choice-making task since they incorporate a spectrum of features
165 that are evaluated based on asymmetric and competing criteria (Malczewski, 2010; Ilugbo et al., 2023b). The
166 combination of these several elements aids in creating a realistic and dependable predictive map that reflects the
167 location's foreseeable groundwater extraction plans. Using multi-criteria decision analysis (MCDA), e.g., AHP, can help
168 accomplish this combination. The AHP is a multifaceted decision-making approach that creates a framework of
169 hierarchy out of an intricate situation—splitting problems into tiers, encompassing objectives, variables, and choices,
170 which are then assessed both intuitively and analytically (Wind and Saaty, 1980; Dar et al., 2021). This approach
171 adequately overcomes the challenge of weight assignment for evaluating indexing; therefore, numerous studies have
172 used the AHP in groundwater potential evaluations (e.g., Singh et al., 2016; Patra et al., 2018; Ajay Kumar et al., 2020;
173 Muthu and Sudalaimuthu, 2021; Dar et al., 2021; Abrar et al., 2021; Zhang et al., 2021; Castillo et al., 2022; Ozegin et
174 al., 2023; Ilugbo et al., 2023a, b; Sharma et al., 2024; Opoku et al., 2024). The proportional relevance of the various
175 objectives is established by a pairwise contrast method that generates a prioritizing scale based on expert judgments
176 (Saha et al., 2024; Opoku et al., 2024). By taking into account a variety of parameters, this method helps analysts
177 establish regions with groundwater potential without being influenced by the geographic environmental spatial
178 complexities (e.g., Dar et al., 2021; Thanh et al., 2022; Baghel et al., 2023). Danumah et al. (2016) employed this
179 approach to identify flood-prone locations, while Akinci et al. (2013), Mansour et al. (2019), Morales and de Vries
180 (2021), Kalura et al. (2021), and Rao et al. (2022) utilized an integrated method that included AHP and GIS to assess
181 the ecological functioning of various regions. In recognition of the intrinsic intricacy and unpredictability of
182 groundwater systems, identifying GWP zones requires the incorporation of multiple data sources into a GIS. A GIS is
183 an effective means for comprehending and inferring geographic information. It can visualize data by processing remote
184 sensing photos, geologic charts, topographic diagrams, and various other kinds of data. This attribute allows for an
185 accurate depiction of the geographical distribution and availability of groundwater supplies (Pande et al., 2020; Baghel
186 et al., 2023). The use of AHP and GIS tools provides an efficient method for conducting quantitative and
187 methodical/systematic evaluations of groundwater potential.
188 This study accentuates the importance of incorporating all-inclusive geospatial (GIS and RS), machine learning (ML),
189 and AHP techniques to establish the GWP zones in a geographical region with a diversity of anthropological (normalized
190 difference vegetation index (NDVI)), hydrogeological (geology and lineament density), hydrological (rainfall
191 distribution and proximity to surface water bodies), and topographical factors (aspect, drainage density, slope, and
192 topographic wetness index (TWI)). The study's objectives are fourfold: (i) to discern and assess the variables that
193 influence groundwater; (ii) to integrate the AHP and ML techniques within a GIS context in order to generate high-
194 accuracy prospective groundwater maps of the research area; (iii) to determine the reliability of AHP and ML
195 technology in determining GWP zones using the AU-ROC curve, guaranteeing a rational system for assessing
196 groundwater potential; and (iv) to leverage cutting-edge geospatial, machine learning, and multi-subjective analysis
197 approaches to offer a useful decision-support system for farming strategy and sustainable use of water resources in the
198 research area. These will support the development of economical, efficient, and scientific approaches to sustainable
199 management of groundwater by water administrators and regulators. The findings of this study may potentially offer
200 sensible suggestions for managing and developing groundwater in regions with complicated geologic origins. Besides,
201 this study advances the domain of geospatial evaluation and environmental modelling by demonstrating the ability of
202 machine learning techniques to resolve difficult hydrogeological concerns while enhancing the management of water
203 assets.
204 The remaining sections of the paper are structured as follows: Section 2 highlights the study area. Section 3 presents the
205 data sources and proposed approaches. Section 4 evaluates and discusses the modelling results, which include
206 experimental appraisal, comparative analysis, model constraints, and a critique of the SDGs' potential consequences.
207 Finally, Section 5 presents important findings, their potential for improvement, and ideas for further investigation.
208
209
210
211
212
213
214

215 **2. Study Area**

216 The research area is situated in Edo North District (sheet 226), Edo State, Nigeria (**Fig. 1**). This area (6°00-6°30E,
217 7°00-7°30N) was selected for its distinct assembly of geographical, meteorological, and demographic factors,
218 making it an appealing perspective for groundwater evaluation in data-scarce areas.

219 According to Odeyemi (1981) and Obaje (2009), the research region is notably located among the Precambrian
220 basement complex rocks of the southwest region of Nigeria, forming part of the Nigerian basement complex and
221 the Pan-African mobile belt, which is located east of the West African Craton. The eastern and western districts
222 are the two separate provinces that make up the basement complex of southwest Nigeria. Migmatite, Gneisses,
223 and substantial amounts of Pan-African Granites, interposed with Mesozoic Younger Granites, are the features
224 that define the eastern province. In contrast, the western province was primarily composed of gneisses or granites,
225 migmatite, and poor-quality Schist Belt. The southwest section of the basement complex in southwest Nigeria
226 constitutes where the research region is located. The rocks in this region are migmatite–gneiss complexes, which
227 are primarily sedimentary series with modest igneous rock incursions believed to have undergone granitic,
228 migmatitic, and metamorphic changes (see Obaje, 2009) over the course of geological history. Considering already
229 existing basic structures were obliterated by succeeding distortion, Odeyemi (1981) proposes that nearly each of
230 the foliations seen in the rocks of southwestern Nigeria, with the exception of intrusives, is primarily tectonic in
231 provenance. The landscape is mostly gently sloping, with granitic mountains extending eastward. Given that the
232 majority of the studied region is fundamentally resistant to groundwater possibility, significant faulting and
233 weathering processes triggered by secondary porosity commonly occur in the availability of groundwater in the
234 studied region. Accordingly, fractures, geologic interactions, shearing regions, faults, and various other
235 discontinuities typically regulate the movement of groundwater in the hard rocks; their complex interactions
236 regulate the process of the watershed as a whole (Ozegin et al., 2023). Groundwater is accessed in a study region
237 through springs, hand-dug wells, and deep reservoirs.

238 The study region is between 46 and 671 meters above sea level. The human population in some parts of the study
239 area is dispersed widely because of the region's rough terrain. The region's climate and vegetation make it easier
240 to grow food crops, including cereals, yams, beans, maize, cassava, plantains, and some tree crops like avocados,
241 mangos, oil palms, and cashews, in addition to a variety of other income crops. Since there are several agrarian
242 community farms in the area, agriculture is the primary occupation of the people living in the studied area.
243 Recognizing that groundwater is the inhabitants' primary supply of potable and irrigation water, it is critical to
244 assess aquifer possibilities in this region. Furthermore, given the region's relatively tropical climate, the
245 development of soil and weathering of rocks are encouraged. Rain and dry conditions are the two basic ones. Low
246 to moderate rainfall occurs throughout the rainy period, which starts in basically April and spans through October.
247 November marks the start of the dry period, which ends in March. The geologic framework controls the relief,
248 which is characterized by lower-lying areas to the south and rising older granites in the uneven hilly higher
249 elevations, especially across the northern margins. In the context of pedology, the research area exhibits saturated
250 loamy and stony sandstone varieties of soil in the western portion, alternating with clayey soil in the eastern
251 portion, which primarily covers the middle and eastern parts.



252

253

Fig. 1. The map depicts the region of focus

254

255

256 **3. Data sources and Methodology**

257 In order to determine the GWP zones in a geographical area located in the Edo North Sub-basin of Nigeria, this
 258 study emphasizes the significance of combining comprehensive geospatial data, ML algorithms, and AHP
 259 techniques. Numerous influencing criteria were used in this evaluation. However, a multicollinearity (MC)
 260 analysis helped narrow down the influencing factors to the nine features subsequently used: normalized difference
 261 vegetation index (NDVI), geology (GY), lineament density (LD), rainfall distribution (RD), proximity to surface
 262 water bodies (PSW), aspect (AP), drainage density (DD), slope (SP), and topographic wetness index (TWI). GWP
 263 zone evaluation and spatial modelling are conducted using data from multiple databases.

264 **Table 1** outlines the geographical data used in the study, indicating the sources that were used. Nine theme layers
 265 were created by combining data from various sources. In the scientific field, thematic layers are an effective
 266 method for establishing potential GW locations. The Shuttle Radar Topography Mission (SRTM) and digital
 267 elevation model (DEM) information were combined to generate distinct geographic features known as the
 268 conceptual strata. These layers comprised lineament density (LD), aspect (AP), drainage density (DD), slope (SP),
 269 and topographic wetness index (TWI). PERSIANN rainfall data from 2021-2024 was leveraged to generate the
 270 rainfall distribution data because the Climatic Research Unit (CRU) has a significantly broader resolution and
 271 consequently provides no detailed resolution for our study area; a geologic map was produced by digitizing the
 272 previous EDO state map (Ozegin and Ilugbo, 2025); and an NDVI map was generated using the MODIS13Q1
 273 dataset retrieved for this date (12-07-2022) and explored from the NASA LAAD DAACS site. PSW was produced
 274 using the topographic map from ArcGIS online digitized. To create maps indicating the potential of groundwater,
 275 a thorough evaluation has been carried out using knowledge-centred weighted analysis and AHP models. This is
 276 a popular method for choosing a decision that incorporates a number of factors (Saaty, 1990). Once the weights
 277 of each class were established, an overlay analysis was performed using ArcGIS's raster calculator. Weights in
 278 AHP were normalized using the geometrical average algorithm. In order to get the geometric mean, the variables
 279 were scored using a predetermined scale (1–9). The geometric average is calculated by dividing the overall scale
 280 weight—the sum of the scales of all the parameters—by a total quantity of variables. Also, machine learning
 281 algorithms, including RF, SVM, AdaBoost, and XGB, were incorporated. The illustration graphic (**Fig. 2**) provides
 282 a detailed representation of the entirety of the processes used in the study.

283
 284
285 Table 1

286 The dataset utilized in the research for GWP categorization modelling.

Factors	The categories of data and formats.	Description	Date last accessed	Source
Geology	Image	Georeferenced	April, 28, 2025	NGSA
Lineament density	SRTM DEM 30m – Raster	Derived from DEM	April, 25, 2025	https://opentopography.org/
Drainage density	SRTM DEM 30m – Raster	Derived from DEM	April, 25, 2025	https://opentopography.org/
Slope	SRTM DEM 30m – Raster	Derived from DEM	April, 25, 2025	https://opentopography.org/
Aspect	SRTM DEM 30m – Raster	Derived from DEM	April, 25, 2025	https://opentopography.org/
Topographic wetness index	SRTM DEM 30m - Raster	Derived from DEM	April, 25, 2025	https://opentopography.org/
NDVI	MODIS 13Q1- Raster	Downloaded	April, 28, 2025	https://ladsweb.modaps.eosdis.nasa.gov/search/
Proximity to surface water bodies	Topographic map – ArcGIS Online	Digitized	April, 29, 2025	ArcGIS
Rainfall	PERSIANN – Raster	Downloaded	2021- 2024	https://chrsdata.eng.uci.edu/
Borehole data	Vector	Derived from detailed fieldwork	April, 19, 2025	Research fieldwork survey

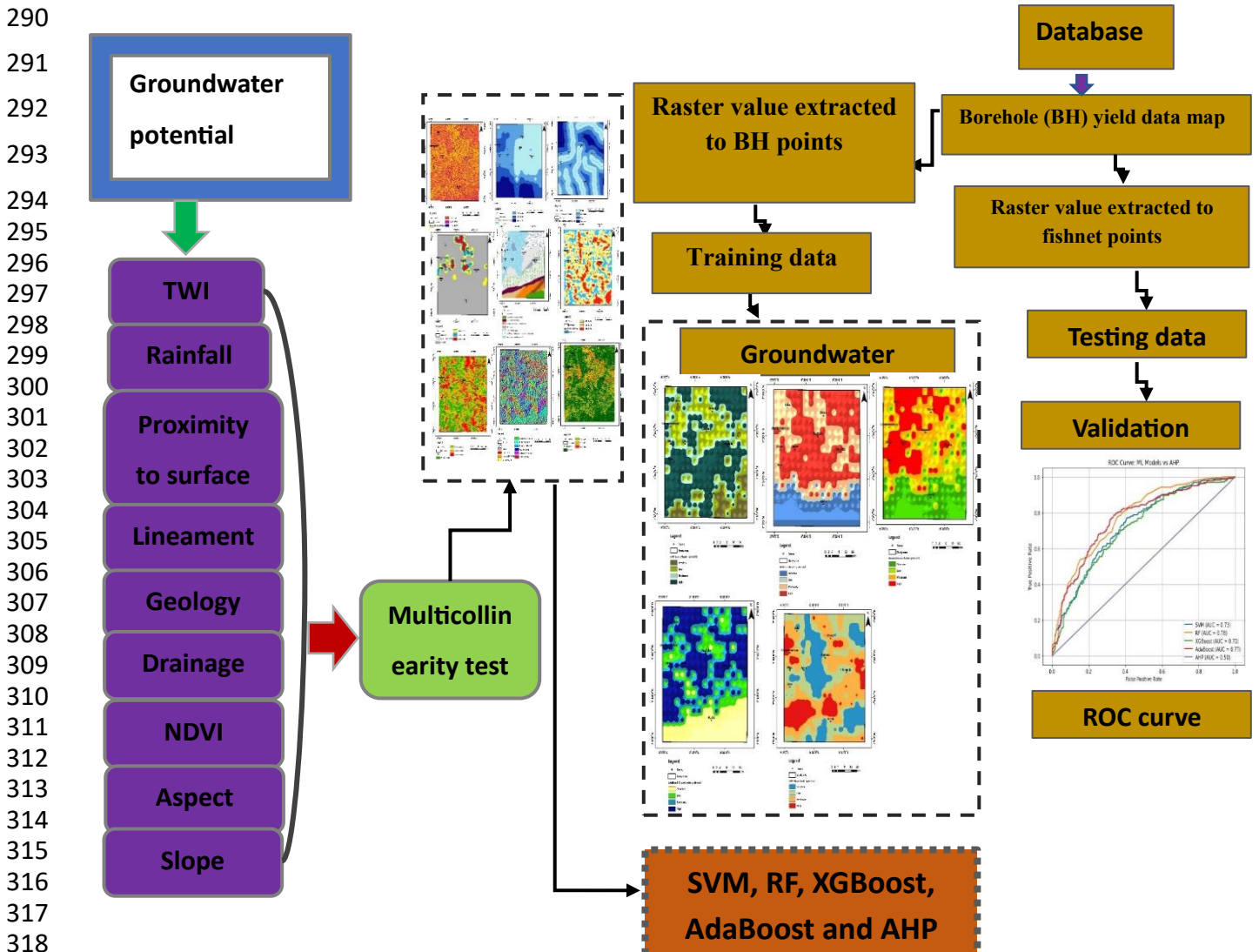


Fig. 2. A flow diagram describing the research's methodology

3.1. Collinearity statistics

To verify the plurality of affecting parameters, collinearity statistical processes were established prior to overlay analysis implementation. A significant correlation between the components can be detected during the multiple regression algorithm analysis; this is known as multicollinearity (MC) (e.g., Venkatesh and Parimalarenganayaki, 2023; Ozegin et al., 2024b). It should be noted that MC evaluations are usually conducted prior to regression studies in groundwater-conceivable models in order to guarantee the accuracy and dependability of the model. Nine (9) groundwater-predicting indicators with a significant effect on freshwater were selected for the study geographic location, and tolerance (T) and variance inflation factor (VIF) served as means to assess the degree of multiple correlations. To avoid distortion in groundwater models, these freshwater-influencing features were to be assessed for MC prior to proceeding with geospatial and ML modelling. Arguably, the leading application of regression in the sciences of hydrology is the development of spatial algorithms that link hydrological parameters, such as estimates of the lowest flow, to water attributes (Kroll and Song, 2013; Ozegin et al., 2024b). Tolerance (T) and variance inflation factor (VIF) were measured using a method known as linear regression in this study to perform collinearity statistics. This approach uses one input characteristic as a variable that depends on the

340 remaining elements as distinct variables in order to determine the coefficient of determination (R^2). The values of
 341 T and VIF are usually determined (e.g., Saha, 2017; Maity and Mandal, 2019; Venkatesh and
 342 Parimalarenganayaki, 2023; Ozegin et al., 2024b) using Eqs. (1) and (2).

$$343 \quad T = 1 - R^2 \quad (1)$$

$$344 \quad VIF = \frac{1}{T} \quad (2)$$

345 The procedure stated above is repeated by modifying the dependent components until the T and VIF are
 346 determined for all factors. T limits are > 0.10 , and VIF is ≤ 10 . A value for each factor that deviates from the
 347 standard values (i.e., $T < 0.10$ and VIF values > 10) shows multicollinearity issues and should be deleted when
 348 evaluating prospective maps (Saha, 2017; Venkatesh and Parimalarenganayaki, 2023; Ozegin et al., 2024b).

349 The ArcMap extraction program was used to determine the values of 500 ($N = 500$) independently selected spots
 350 within the theme maps for the determinants' convergence statistics. T and VIF values were computed in **Table 1**
 351 after a linear regression examination was carried out using the statistical package SPSS on the obtained
 352 parameters.

353 3.2. MCDA-AHP-based model and GIS techniques

354 3.2.1. AHP for GWP (Comparative matrix development and variable weighting)

355 The AHP framework, among the MCDA-based frameworks employed to provide outcomes for difficult decision-
 356 making scenarios, was initially developed by Saaty (1990). One widespread MCDA process for addressing natural
 357 assets and the surrounding ecosystem is Saaty's (1990) AHP. Applying the widely utilized AHP approach, a
 358 standardized weight is assigned to each theme layer of the groundwater exploring feature. The principal
 359 eigenvalue of the generated matrix was used to determine the final weight for every theme layer. The relative
 360 weights and correlations of every item are examined in the first step of AHP computations using an $n \times n$ matrix
 361 (A) with diagonal parts equal to 1. As the comparison of pairs demonstrates, the value is additionally adjusted to
 362 get a weighted value (W). The foundation of the concept of AHP is a set of paired assessing matrix equations (Eq.
 363 3) that compare encompassing factors in order to assess the weighting of every parameter (see Saaty, 1990; Das,
 364 2019; Abrar et al., 2021; Ozegin et al., 2023; Ilugbo et al., 2023a; Baghel et al., 2023; Sharma et al., 2024; Zewdie
 365 et al., 2024). The most prevalent method for identifying the prioritizing vector is the Saaty technique, which asserts
 366 that the most important vector should be the dominating eigenvector of A. Given the homonymic idea, it is
 367 frequently called the Perron-Frobenius eigenvector in an algebraic linear relationship (Horn and Johnson, 1985;
 368 Brunelli, 2015; Ozegin et al., 2024a, b, c). The following realization forms the foundation of the process: Eq. (3)
 369 can be obtained by multiplying a matrix A by W along with its entries, which are exactly expressed as weighted
 370 proportions:

$$371 \quad AW = \begin{bmatrix} 1 & a_{12} & a_{13} & \cdots & a_{1n} \\ 1/a_{21} & 1 & a_{23} & \cdots & a_{2n} \\ 1/a_{31} & 1/a_{32} & 1 & \cdots & a_{3n} \\ \vdots & \vdots & \vdots & \ddots & \vdots \\ 1/a_{m1} & 1/a_{m2} & a_{m3} & \cdots & 1 \end{bmatrix} \begin{bmatrix} w_1 \\ w_2 \\ w_3 \\ \vdots \\ w_n \end{bmatrix} \quad (3)$$

372 A comparison is made between the row matrices and column matrices components. Skilled competence, actual
 373 fieldwork, and the possible influence of groundwater were used to determine the proportions of all of the distinct
 374 strata. In this research, the pairwise evaluation phase of the AHP technique was conducted using a 9×9 matrix.
 375 **Table 2**'s comparative ratings, which are determined on Saaty's 1 to 9 scale, were developed using knowledgeable
 376 views and assessments of pertinent literature to determine the relative value of each influencing feature for
 377 explorative characteristics. According to the Saaty scale, utmost significance is represented by a number of 9, high
 378 significance by a number of 7, great by a value of 5, considerable by a number of 3, equally significant by a value
 379 of 1, and intermediary significance by a number of 2, 4, 6, and 8. According to the categorization, themes are
 380 given weights according to their importance and ability to retain water. A pairwise evaluation matrix was used for
 381 contrasting the influencing variables (**Table 3**). The comparative comparison's outcome is adjusted to establish
 382 each parameter's score. To generate a diagonally oriented matrix, Saaty (1990) recommends aligning the numbers
 383 in the matrix's top triangle. The inverse values of the originating array are then inserted into the base triangular
 384 array. The proportional weights produced by this procedure are then established (**Table 4**). An estimate of the
 385

proportionate relevance of the indicators being compared is given by these averages. The final indicator priority is represented by the normalized quantities of the eigenvectors, which are linked to the optimum eigenvalues of the proportionate (ratio) matrix. The process outlined here constitutes the most effective way to lessen the impacts of ratio inequalities. Corresponding values of the criteria are shown in **Table 5**. The dominant geological characteristics and intricate recharge mechanisms describe this research locale.

The principal eigenvalue, which evaluates the uniformity of the approach to decision-making, is used to compute the consistency ratio (CR). The CR aids in assessing the consistency and dependability of the decisions reached when comparing the criteria by pairing.

Table 2:

Scale for value in relative terms.

Strength	1	3	5	7	9	2,4,6,8
Description	equally significant	considerable	great	highly significant	utmost significance	Intermediary significance

Table 3.

Comparative matrix between pairings with the primary eigenvector normalized.

Matrix	TWI	RD	PSW	LD	GY	DD	NDVI	AP	SP	Primary eigenvector normalized
TWI	1.000	0.500	2.000	0.500	0.333	1.000	3.000	5.000	5.000	10.5554%
RD	2.000	1.000	3.000	1.000	0.500	2.000	5.000	7.000	7.000	17.9395%
PSW	0.500	0.333	1.000	0.333	0.250	0.500	2.000	4.000	4.000	6.8214%
LD	2.000	1.000	3.000	1.000	0.500	2.000	5.000	7.000	7.000	17.9395%
GY	3.000	2.000	4.000	2.000	1.000	3.000	6.000	8.000	8.000	27.3092%
DD	1.000	0.500	2.000	0.500	0.333	1.000	3.000	5.000	5.000	10.5554%
NDVI	0.333	0.200	0.500	0.200	0.167	0.333	1.000	3.000	3.000	4.3478%
AP	0.200	0.143	0.250	0.143	0.125	0.200	0.333	1.000	2.000	2.4456%
SP	0.200	0.143	0.250	0.143	0.125	0.200	0.333	0.500	1.000	2.0862%
Summation										100%

Normalized difference vegetation index (NDVI), geology (GY), lineament density (LD), rainfall distribution (RD), proximity to surface water bodies (PSW), slope (SP), drainage density (DD), topographic wetness index (TWI) and aspect (AP).

Table 4.

Normalized matrix

	TWI	RD	PSW	LD	GY	DD	NDVI	AP	SP
TWI	0.103678	0.10556	0.103379	0.10556	0.108488	0.103678	0.103807	0.106946	0.108891
RD	0.178193	0.1772	0.180328	0.1772	0.178413	0.178193	0.180942	0.182827	0.181259
PSW	0.067383	0.06975	0.064904	0.06975	0.072326	0.067383	0.064497	0.066985	0.070948
LD	0.178193	0.1772	0.180328	0.1772	0.178413	0.178193	0.180942	0.182827	0.181259
GY	0.278818	0.27207	0.281312	0.27207	0.260372	0.278818	0.281803	0.271214	0.261351
DD	0.103678	0.10556	0.103379	0.10556	0.108488	0.103678	0.103807	0.106946	0.108891
NDVI	0.043209	0.045112	0.041115	0.045112	0.047179	0.043209	0.04004	0.041084	0.045243
AP	0.025152	0.025885	0.02398	0.025885	0.025873	0.025152	0.023193	0.021796	0.023186
SP	0.021695	0.021662	0.021275	0.021662	0.020448	0.021695	0.02097	0.019375	0.018971

411
412**Table 5.**
Evaluation of input parameter weights and classification for GWP zoning

Criteria	Prospect for groundwater potential	Class	Area covered (Km ²)	% of the study area covered	Rating	Normalized AHP Weight
TWI	Maximum value preferred	-0.782 – 3.371	905	38	1	0.10555
		3.372-5.41	970	41	2	
		5.411-8.733	385	16	3	
		8.734 – 18.475	130	5	4	
	Total		2390	100		
RD (mm/year)	Maximum value preferred	2104 – 2,339	808	34	1	0.17940
		2340 - 2446	767	32	2	
		2447 – 2579	418	17	3	
		2580 – 2767	397	17	4	
	Total		2390	100		
PSW (km)	Minimum value preferred	High	888	37	1	0.06821
		Moderate	872	36	2	
		Low	330	14	3	
		Very low	300	13	4	
	Total		2390	100		
LD (km⁻¹)	Maximum value preferred	0 – 0.090	1988	83	1	0.17940
		0.091 – 0.270	192	8	2	
		0.271 – 0.500	130	5	3	
		0.501 – 0.860	80	4	4	
	Total		2390	100		
GY	Type descriptive	Clays, shales with limestone	590	25	3	0.27309
		Coal, sandstone and shale	419	18	2	
		Falsebedded sandstone, coal and shale	505	21	1	
		Older granite	352	15	3	
		Shale and mudstones	265	11	4	
		Undifferentiated basement complex with pebbles	149	6	3	
	Total		2390	100		
DD (km⁻¹)	Minimum value preferred	0.030 – 0.750	515	22	4	0.10555
		0.751 – 1.060	746	31	3	
		1.061 – 1.380	703	29	2	
		1.381 – 2.330	426	18	1	
	Total		2390	100		
NDVI (%)	Maximum value preferred	0.0184 – 0.2684	774	32	1	0.04348
		0.2685 – 0.4723	604	25	2	
		0.4724 - 0.6993	601	25	3	
		0.6994 – 0.9993	411	18	4	
	Total		2390	100		
AP (°)	Type descriptive	Flat (-1 - 0)	211	9	4	0.02446
		North (0 – 22.5)	213	9	4	
		Northeast (22.6 – 67.5)	221	9	3	
		East (67.6 – 112.5)	261	11	2	
		Southeast (112.6 – 157.5)	287	12	1	
		South (157.6 – 202.5)	294	12	1	
		Southwest (202.6 – 247.5)	255	11	1	
		West (247.6 – 292.5)	224	9	2	
		Northwest (292.6 – 337.5)	214	9	3	
	Total		2390	100		
SP (°)	Minimum value preferred	0 - 4.0	590	25	4	0.02086
		4.1 – 10.0	100	4	3	
		10.1 – 19.0	700	29	2	
		19.1 – 65.0	1000	42	1	
	Total		2390	100		

413

414

3.2.2. Matrix consistency evaluation

Considering the ratings were based on opinionated or individualized appraisals, they might be somewhat skewed and unpredictable. Therefore, using Eq. 4, the consistency ratio (CR) is typically employed to verify the choice to compare thematic layers and subcategories among conceptual layers by pairing (Saaty, 1990). For the analytical process to proceed, a CR of 0.10 or less is deemed suitable. It is necessary to reevaluate the evaluation considering the CR value exceeds 0.10 in order to identify any sources of inconsistencies and make the necessary corrections. On the other hand, when the CR value is zero, it indicates that the pairwise analysis is perfectly consistent. Moreover, the proportions of weight acquired from this approach were normalized using Table 4. The basic eigenvalue generated in this process is used to evaluate the cohesiveness of conceptions using the CR. Brunelli

(2015) defines the major eigenvalue as the measure of the matrix's deviation from regularity. The CR is calculated by applying **Eq. (5)** with the CI.

$$CR = \frac{CI}{RI} \quad (4)$$

where RI defines random index and CI for consistency index.

$$CI = \frac{\lambda_{\max} - n}{n-1} \quad (5)$$

where n is the variety of features used and λ_{\max} is the principal eigenvalue.

In the context of **Eq. 5**, λ_{\max} denotes the most substantial absolute eigenvalue of the contrasting matrix pairings determined by **Eq. (6)**. (e.g., Ikrri et al., 2023).

$$\lambda_{\max} = \frac{1}{n} \sum_{W_i}^n \frac{(AW)_i}{W_i} \quad (6)$$

In **Eq. (3)**, W is the appropriate eigenvector for λ_{\max} , and AW_i ($i = 1, 2, 3, \dots, n$) is the weighting quantity for every variable, which is conveniently derived from the matrix (Mandal et al., 2021; Ikrri et al., 2023).

Consequently, the CI for the present analysis is

$$CI = (9.22 - 9) / (9 - 1) = 0.0275$$

The dependability of the outputs was evaluated by applying the computed CI and RI values derived from **Table 6** data equivalent to nine (9) in number (Saaty, 1990).

Thus,

$$CR = \frac{0.0275}{1.45} = 0.0190 (1.90\%)$$

The CR, estimated as 0.019 and established to be less than 0.1, showed the resulting weights acquired were uniform (**Table 7**). As a result, the weights established in **Table 5** can potentially be utilized.

Table 6.

RI estimates distinct matrix sizes (Alonso and Lamata, 2006; Ozegin et al., 2024a).

n (matrix size)	1	2	3	4	5	6	7	8	9	10	11	12	13	14	15
RI	0.00	0.00	0.53	0.88	1.11	1.25	1.34	1.41	1.45	1.49	1.51	1.54	1.56	1.57	1.58

Table 7.
Consistency assessment

λ_{\max}	n	RI	CL	CR	Reliability
9.22	9	1.45	0.0275	0.0190	Less than 0.1

3..2.3. The integration of thematic layers to identify groundwater potential zones

The GWPZ, a devoid-of-dimensions measure that represents possible groundwater zones within a given geographical area, was calculated using a weighted linear framework approach, as described by Venkatramanan et al. (2019) and Ozegin et al. (2023). The GWP zones in the study area were determined by a rigorous approach. This procedure incorporated details from nine various themes and used an overlay analysis mechanism within the GIS platform, as well as hybrid weights produced using AHP, as shown in **Eq. 7**.

$$GWPZ = \sum_{i=1}^n W_i x R_i$$

i.e.,

467 $GWPZ = NDVw_iNDVr_i + GYw_iGYr_i + LDw_iLDr_i + RDw_iRDr_i + PSWw_iPSWr_i + APw_iAPr_i + SPw_iSPr_i + DDw_iDDr_i + TWw_iTWr_i \quad (7)$

468

469 GWPZ: groundwater potential zones, where the subscripts w and r reflect the weights and rank value of every
 470 variable, respectively. Every theme layer has a weight (Wi), and the rank of its subcategories is represented by Ri.
 471 The locations were divided into five categories predicated on their probable groundwater zones: very low, low,
 472 moderate, high, and very high.

473

474 3.2.4. Sensitivity analysis (SA)

475

476 Sensitivity analysis is the activity of analyzing the influence of alterations to input data or model variables on
 477 spatial outputs in GIS. SA is an important GIS tool for assessing the integrity and robustness of geographical
 478 frameworks since it can identify areas of ambiguity and potential shortcomings in analysis (Mukherjee and Singh,
 479 2020; Ozegin and Ilugbo, 2025). SA is usually carried out on indicator weights to assess the strength and reliability
 480 of a decision resolution after modifying the weights for a preset set of parameters among options and reconsidering
 481 each of the possible ranks. This enables an organized evaluation of the influence of alterations to criteria weights
 482 on different rank orders. The SA is applied in this study to assess the uniformity of the effects, and it serves as the
 483 foundation for a suitable appraisal of the GWP zone map. It also helps to comprehend the consequences of all of
 484 the parameters employed in GIS-AHP.

485 Map removal SA is an effective tool for determining the significance of various maps or sets of maps in spatial
 486 evaluation. The comparative significance of distinct components might be analyzed, and the quality of their
 487 geographical analysis improved by systematically removing different maps or groups of maps while contrasting
 488 the findings. The SA study was designed to determine the exactness of the prospective groundwater outcomes and
 489 to evaluate effectively all nine (9) criteria that quantify groundwater potential appropriateness. **Table 8** shows the
 490 formula adopted to determine the exactitude of the groundwater potential map.

491

492 **Table 8**

493 Sensitivity analysis equation

Sensitivity analysis	Formula	Description
Map removal	$SI = \frac{\left(\frac{GWPZ}{N} \right) - \left(\frac{GWPZ'}{n} \right)}{GWPZ} \times 100$	<p>where</p> <ul style="list-style-type: none"> ▪ N and n are the number of components considered in the creation of the GWPZ and GWPZ' maps, respectively. ▪ GWPZ denotes the groundwater potential zone created by combining all thematic layers. ▪ GWPZ' denotes the groundwater potential zones created by deleting one thematic layer. ▪ SI represents sensitivity index.

494

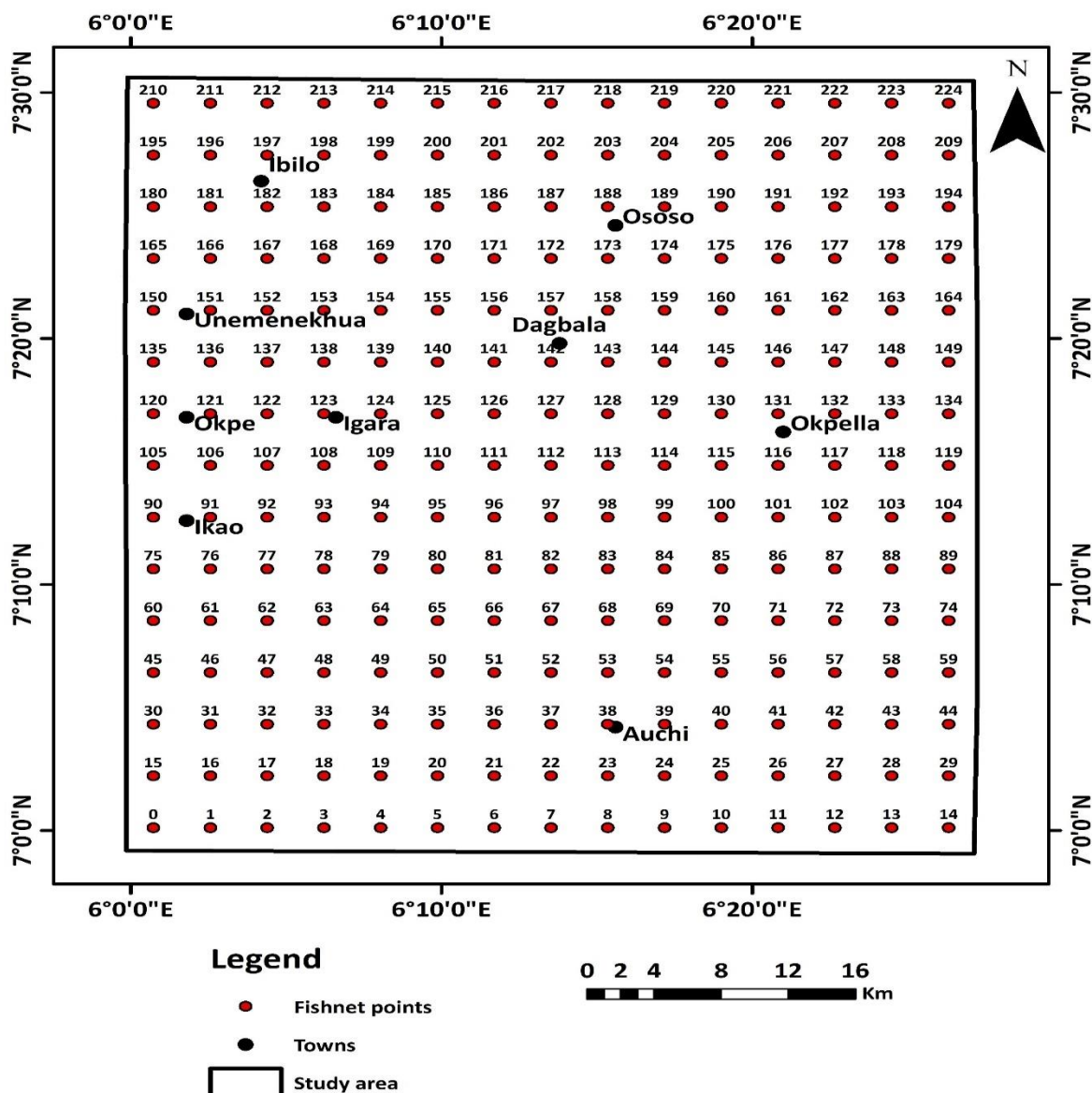
495 3.3. Data preparation for ML models

496 3.3.1. Transforming parameterized values to points

497 The number of training and testing/prediction datasets must be considered before separating the datasets for the
 498 training and testing task so as to use the ML models for the purpose of groundwater potential modelling (Lee et
 499 al., 2020). The main limitation in applying ML is the dearth of sufficient data for training (Hutchinson et al. 2017;
 500 Khan et al. 2021). This difficulty can be overcome by using the 'CreateFishnet_management' before applying the
 501 'ExtractValueToPoint' syntax in ArcGIS (e.g., Khan et al. 2021). A 3×3 -meter grid (**Fig. 3**) was formed on all of
 502 the nine water raster layers (based on the nine-layer theme utilized in the study), and 224 grid points' raster values
 503 were retrieved. These grids are rectangular or square cells, resembling a fishnet (FN), hence the name. Fishnets
 504 are a type of grid that we use to overlay a feature on a map. It is used for organizing spatial data into manageable,
 505 comparable units. This segmentation allows users to aggregate data within each cell. To train the ML models, a
 506 new technique was used because the study area contained minimal borehole (BH) data (i.e., 36). This method

507 involves training the models with 100% BH data (i.e., target indicator) and then utilizing the trained model for
 508 predicting 100% of the variables serving as predictors, which were designed to be completely hidden from the
 509 models during the training process. To implement this technique, raster values of the estimating variables
 510 were taken to the BH location points. The multiple classes designated BH data (i.e., low (0), moderate (1), and
 511 high (3)) were utilized for model training. Also, the raster values of indicators extracted to the 224 fishnet
 512 locations (**Fig. 3**) created using the fishnet development tool in ArcGIS 10.7 software were applied as the
 513 forecasting parameters. This approach provides a simple yet reliable mechanism for applying ML models to
 514 geospatially scarce target variable data locations.

515 A borehole yield map will be created to evaluate the classification evaluation criteria specified, and fishnet points
 516 will be retrieved from the drill yield data. This categorization was subsequently contrasted with the kind of
 517 classification projected by all of the ML models, yielding the AUC-ROC.
 518



519

520 **Fig. 3.** The Fishnet developed for the research region to extract values from a raster layer.
 521

522 3.3.2. Random forest (RF)

523 RF is a controlled ML algorithm that builds a collection of categorization trees derived by the randomized
 524 sampling of a cluster of features from the variable space and a bootstrap process that repeatedly picks a fraction
 525 of the input platform to adapt the model. It is an additional powerful and effective ML algorithm that was designed

526 by Breiman (2001) as a further development of the "classification and regression trees" to increase its capacity
 527 for predicting competency (Razavi-Termeh et al., 2019; Maskooni et al., 2020). Diverse decision trees are
 528 generated using randomized bootstrapped calibrated sets (Breiman, 2001). The model then incorporates the mean
 529 results from every tree (Moghaddam et al., 2020). The individual performing the operation is required to choose
 530 two parameters, namely "the number of variables at each split" and "the number of trees" (Razavi-Termeh et al.,
 531 2019). This model does not employ the entire data set to create the tree; it only uses 66.66% of the bootstrap data.
 532 Subsequently, 33.33% of the other information is employed to assess the suited tree. In the present study, the
 533 framework was carried out in R using the 'randomForest' program (Liaw and Wiener, 2024). As a result of its
 534 dependable and efficient productivity, it is commonly used as a tree-based ML algorithm to study the complex
 535 link between groundwater-influencing features (Hasanuzzaman et al., 2022; Shandu and Atif, 2023). The model
 536 uses an identical generating approach as classification and regression trees (CART), but it creates multiple trees,
 537 resulting in a "forest" (Wiesmeier et al., 2011). It is capable of handling data from a variety of measurements
 538 without making mathematical suppositions (Rahmati et al., 2016). The RF model is famous because it is capable
 539 of addressing what is termed as the "black box," which frequently serves as a shortcoming of ML approaches,
 540 including ANN, and it is sturdy in dealing with outliers (e.g., Shandu and Atif, 2023). It provides explanations for
 541 connection and nonlinear correlations among components (e.g., Naghibi et al., 2016).

542 The covariance and variance that exist across grid cells can be determined by utilizing out-of-bag (OOB) error
 543 data (McKay and Harris, 2016; Naghibi et al., 2016). The bootstrap samples are then used to anticipate the missing
 544 OOB samples, and the mean square error (MSEOOB) is calculated by summing the OOB projections from the
 545 entire model trees (Wiesmeier et al., 2011; Prasad et al., 2020). **Eq. 8**, which integrates the mean square error of
 546 every model decision tree with its associated OOB samples for appraisal, was used to get the learning error Eoob.
 547 These features represent an estimation of ambiguity surrounding the assessment of prospective groundwater at a
 548 grid cell.

549

$$550 \quad E_{OOB} = \frac{1}{2} \sum_{i=1}^n (y_i - \hat{y}_i)^2 \quad (8)$$

551 The total number of OOB samples is denoted by "n," the obtained outcome by y_i , and the model result from RF
 552 produced during training by \hat{y} (Prasad et al., 2020). The mean across the trees is the model's outcome (Rahmati
 553 et al., 2016).

554

555 3.3.3. Support vector machine (SVM)

556

557 SVM is a controlled ML algorithm that is implemented using the structural risk minimization (SRM) concept and
 558 theoretical framework of statistical learning (e.g., Tehrany et al., 2015; Kavzoglu et al., 2019). SVM converts the
 559 initially provided input field into a feature space with greater dimensions in order to locate the best segmenting
 560 hyperplane. Marjanović et al. (2011) confirmed that a hyperplane that separates is formed in the initially created
 561 space of n dimensions between vertices from two independent classifications. If the location lies above the
 562 hyperplane, it is designated as +1; otherwise, it is labelled as -1. It is often used to resolve classification and
 563 regression difficulties, reducing algorithmic excessive fitting (Gayen et al., 2019).

564 When addressing linearly separable data, **Eq. 9** is easily used to calculate a separating hyperplane (Hong et al.,
 565 2017):

566

$$567 \quad y_i(w \cdot x_i + b) \geq 1 - \xi_i \quad (9)$$

568 The coefficient vector w indicates the hyperplane's inclination in the characteristic space, whereas b is the
 569 hyperplane's distance from its starting point, and ξ_i determines the positive slack components. **Eqs. 10a** and **b**:
 570 The optimization problem is potentially addressed by establishing an ideal hyperplane (Samui, 2008).

571

$$572 \quad \text{Minimize } \sum_{i=1}^n a_i - \frac{1}{2} \sum_{i=1}^n \sum_{j=1}^n a_i a_j y_i y_j (x_i \cdot x_j) \quad (10a)$$

$$573 \quad \text{Subject to } \sum_{i=1}^n a_i y_i = 0, 0 \leq a_i \leq C \quad (10b)$$

574 In this case, C stands for the penalty and a_i for the Lagrange multiplier. The choice of kernel format affects the
 575 SVM model's accuracy of efficient categorization (Yao et al., 2008). Many scholars (e.g., Tehrany et al., 2015;
 576 Gayen et al., 2019) have claimed that the radial basis function (RBF) has a stronger interpolation effectiveness,
 577 which is why it was used in this study. Eq. 11 typically defines how RBF can be determined:

$$RBF: K(x_i, x_j) = \exp(-\gamma x_i - x_j^2) \quad (11)$$

579 where the RBF kernel function is denoted by y and the kernel function by $K(x_i, x_j)$. Using the technique was
 580 intended to lower the model's complexity and inaccuracy (Naghibi et al., 2018). The composite model emerged
 581 by merging two or more distinct prediction models.
 582

583 3.3.4 Adaptive boosting (AdaBoost)

584 3.3.4. Adaptive boosting (AdaBoost)
585 Adaptive boosting is an efficient composite learning approach that updates the weight of training scenarios to
586 fully use a restricted number of instances for learning. After every round of weak learners, the AdaBoost method
587 maintains a set of values and adjusts them to create poor learners within the training dataset (e.g., Freund and
588 Schapire 1995, 1997). All weights get configured uniformly at the start. In each cycle, the weight of the
589 appropriately categorized samples decreases, whereas the weight of the samples that were misidentified increases.
590 However, this boosting technique does not require previous experience of the efficacy of the weak algorithm in
591 operation (Jennifer, 2022).

592 The starting weights for every sample are assigned at the start of each step using the formula $\omega_i^{(1)} = \frac{1}{N}$, where N
 593 is the number of evaluations. After training the weak discriminant h_t with weights $\omega_i^{(t)}$ on the training collections,
 594 the weighted error (err_t) and discriminant weight (a_t) are calculated (Eqs. 12a and b).

$$595 \quad err_t = \frac{\sum_{i=1}^N \omega_i^{(t)} \cdot I(y_i \neq h_t(x_i))}{\sum_{i=1}^N \omega_i^{(t)}}, \quad (12a)$$

$$596 \quad \alpha_t = \frac{1}{2} \cdot \log \log \left(\frac{1 - err_t}{err_t} \right) \quad (12b)$$

597 In this instance, t is a number between 1 and T , while T is the total quantity of repetitions. y_i represents the real
 598 classification label of input i , $h_t(x_i)$ represents the assumption made by the t th weak classifier for the identical
 599 sample, and $\omega_i^{(t)}$ is the weight given to the sample at repetition t . In the case of an incorrect classification, where
 600 the real label is different from the label anticipated by the weak classifier, the indicating functions $I(y_i \neq h_t(x_i))$
 601 equate to 1.

At every round t , the algorithm (AdaBoost) determines the weighted error and total weight of the weak classifier before updating the sample weighting. In order to focus the next iterations on cases that the existing ensembles of inadequate classifiers were incapable of sufficiently training, the modification aims to give the wrongly categorized samples bigger weights. The sample weight adjustment is expressed using Eq. 13:

$$606 \quad \omega_i^{t+1} = \omega_t^{(t)} \cdot \exp\exp(-\alpha_t \cdot y_i \cdot h_t(x_i)) \quad (13)$$

607 Integrating the weak classifiers yields the ultimate predictions for the binary category issue (**Eq. 14**):

$$608 \quad H(x) = sign\left(\sum_{t=1}^T \alpha_t \cdot h_t(x) \right) \quad (14)$$

609 The projection made by the t th poor classifier given a sample is represented by $h_t(x)$ in this expression. The
 610 ultimate projection is guaranteed to be between +1 and -1, signifying the +ve or -ve categories, respectively, due
 611 to the sign () operator.

613 3.3.5. eXtreme gradient boosting (XGB) algorithm

615 The XGB technique is a sophisticated gradient boosting solution developed for machine learning assignments that
 616 require great rapidity and effectiveness. It implements visual illustrations to assess preference answers and
 617 expands upon decision tree approaches. By arbitrarily selecting attributes to create a forest of trees, XGB's bagging
 618 combination approach improves predictability by combining forecasts from several decision trees by dominant
 619 voting. The basic premise is simply to construct classification or regression trees one at a time, then train the next
 620 model using the remaining data from the prior tree. To improve the training operation, this approach can use values
 621 from already trained trees (e.g., Niazkar et al., 2024). By eliminating decision points that make minimal
 622 contributions to goal values, the pruning process minimizes the size of a decision tree and helps prevent
 623 overfitting. Even with values not present in the datasets, XGB performs more efficiently.

624 The XGB and AdaBoost approaches constitute part of the collaborative learning framework, which involves
 625 training weak learners sequentially to generate an effective model. In comparison to AdaBoost's concentration on
 626 deciding on a stump for weak learners, XGB takes a more adaptable strategy, regularly employing decision trees
 627 and incorporating normalization algorithms to thwart excessive fitting (**Eq. 15**).

$$628 F(X) = \sum_{m=1}^M f_m(X) \quad (15)$$

629 In this instance, every weak learner's aggregate input results in the ultimate projection $F(X)$, which is represented
 630 as $f_m(X)$, where M is the entire set of weak learners. By deliberately training a single tree to minimize the
 631 diminution of its predecessors, a method of adaptation is created that raises the accuracy of the entire model. The
 632 incorporation of regularity elements into the objective function is a crucial element in XGB's effectiveness.
 633 Regularity in XGB is accomplished by the use of penalty features in the objective function, which is composed
 634 of two fundamental parts: the term that regulates and prohibits overwhelmingly complicated models and the loss
 635 term that evaluates how well the model matches the training data. **Eq. 16** provides the following expression for
 636 the objective function:

$$637 Obj = \sum_{i=1}^n L(y_i, \hat{y}_i) + \sum \Omega(f_m) \quad (16)$$

638 $\Omega(f_m)$ represents the regularization term given to the m th tree, and $L(y_i, \hat{y}_i)$ represents the loss function, which
 639 quantifies the difference between the true label (y_i) and the anticipated label (\hat{y}_i).

640 3.4. Model performance evaluation

641 The verification of every model is an essential phase in empirical research (Naghibi et al., 2016; Ozegin et al.,
 642 2024a, b, c). Evidently, there are numerous methods for determining the performance of MLAs, notably the
 643 ROC curve, considered an accurate depiction of how effectively the algorithms perform, particularly in binary
 644 categorization tasks (Sachdeva and Kumar, 2021; Singha et al., 2024; Rana et al., 2025). The graph plots a
 645 classifier's accuracy leveraging the true positive rate (TPR) vs. the false positive rate (FPR) at various threshold
 646 settings. The horizontal represents TPR, often known as sensitivity or recollection (**Eq. 17a**). It refers to the ratio
 647 of the number of reliably anticipated observed positives to the entire number of occurrences in the real class.
 648 Nevertheless, FPR, calculated as (1—specificity) and plotted on the horizontal axis (**Eq. 17b**), estimates the
 649 fraction of incorrectly expected positive findings compared with the total number of real negative evaluations
 650 (Prasad et al., 2020; Saha et al., 2022). TN depicts true negative, FP means false positive, TP means true positive,
 651 and FN means false negative (Bai et al., 2022; Braham et al., 2022).

$$652 Y = \text{sensitivity} = \left[\frac{TN}{(TP + FN)} \right] \quad (17a)$$

653
$$X = 1 - specificity = 1 - \left[\frac{TN}{(TN + FP)} \right] \quad (18b)$$

654 The receiver operating characteristic (ROC) curve was used to analyze the GWP map's performance across various
 655 techniques. The area under the receiver-operating characteristic (AU-ROC) curve is often employed for assessing
 656 model prediction capacity, with a greater AUC indicating a superior model (Rahmati and Melesse, 2016;
 657 Echogdali et al., 2022). The area under the receiver-operating characteristic (AU-ROC) curve, often known as the
 658 area under the curve (AUC), was calculated to assess the reliability of predictions.

659 According to Senapati and Das (2021) and Ozegin et al. (2024b), the AUC values varied from 0 to 1 (**Table 9**).
 660 While a number of 0 denotes no difference between the likelihood of groundwater (weak relationship) and the
 661 available data, a value of 1 denotes the highest degree of accuracy (e.g., Masroor et al., 2023; Ali et al., 2023;
 662 Ozegin et al., 2024b; Sharma et al., 2024). A high ROC value suggests that the model is very effective.

663 **Table 9.**

664 AUC values

S/No.	Range	Description
1.	0.50–0.60	poor
2.	0.61–0.70	average
3.	0.71–0.80	good
4.	0.81–0.90	very good
5.	0.91–1.00	excellent

665 **4. Results and discussion**

666 The study of geospatial evaluation of geological features is critical to determining where and what dimensions of
 667 things are, as well as how they connect to one another. This study is critical for the incorporation of field data and
 668 the generation of various conceptual layers regarding the environment using GIS platforms and remote sensing.
 669 These data sets are merged and leveraged to adequately identify the GWP zone and aid in long-term water asset
 670 development, planning, and administration. The choice of decisive variables is determined by the anthropological,
 671 hydrogeological, hydrological, and topographical characteristics, as well as the accessibility of appropriate data
 672 for the study area. As a result, in this study, the GWP zone map is generated from nine (9) thematic maps:
 673 normalized difference vegetation index (NDVI), geology (GY), lineament density (LD), rainfall distribution (RD),
 674 proximity to surface water bodies (PSW), aspect (AP), drainage density (DD), slope (SP), and topographic
 675 wetness index (TWI). These maps and their particular attributes are extremely important since they indicate the
 676 geographical effect on GW distribution. The study aims to estimate GWP zones in the Edo North district using
 677 AHP and machine learning (ML) methods such as RF, SVM, AdaBoost, and XGB. The subsequent subsections
 678 provide insights on each concept map related to freshwater potential for the present work.

679 **4.1. Variables influencing groundwater multicollinearity evaluation**

680 Seven (7) of the sixteen (16) groundwater-predicting indicators considered in the study exhibit multicollinearity
 681 (**Table 10a**). The statistics identified seven influencing factors with collinearity issues: land use/land cover (LL),
 682 soil type (ST), geomorphology (GM), elevation (EL), ruggedness index (TRI), soil permeability (SB), and stream
 683 power index (SPI). The VIF and tolerance metrics for the aforementioned variables are larger than 10 and less
 684 than 0.1, respectively, and hence were rejected for the development of the various models utilized in the study.
 685 And the following parameters (as demonstrated by T and VIF values > 0.1 and < 10 , respectively) were
 686 subsequently used for the modelling (**Table 10b**), viz., normalized difference vegetation index (NDVI), geology
 687 (GY), lineament density (LD), rainfall distribution (RD), proximity to surface water bodies (PSW), aspect (AP),
 688 drainage density (DD), slope (SP), and topographic wetness index (TWI).

689 The statistical results show that RD possesses the least T value (0.1496) and the largest VIF value (6.6860).
 690 Conversely, LD has the greatest T value of 0.6608 and the smallest VIF score of 1.5132. In the other groundwater-
 691 influencing parameters, the values of T and VIF were observed to lie between RD and LD, as shown in **Table**
 692 **10b**. Consequently, the outcomes demonstrated that there was indeed no evidence of MC among the chosen
 693 indicators, and no ambiguity was infused into the model's outcomes due to the issue of multicollinearity.
 694 Therefore, the assessments show that each of the parameters chosen had an effect on the GWP zones;
 695 consequently, all of these criteria (see **Table 10b**) were incorporated in the modelling process.

699
700
701**Table 10a.**
MC statistics (T and VIF) of the groundwater potential-influencing determinants

S/NO	Criteria	VIF	T
1.	<i>LL</i>	16.4885	0.0606
2.	NDVI	2.1910	0.4564
3.	GY	2.2275	0.4489
4.	<i>ST</i>	13.214	0.0712
5.	LD	1.5132	0.6608
6.	RD	6.6860	0.1496
7.	PSW	2.2299	0.4485
8.	SP	1.6540	0.6046
9.	<i>GM</i>	11.375	0.0787
10.	DD	2.6276	0.3806
11.	<i>EL</i>	<i>infinity</i>	<i>infinity</i>
12.	TWI	3.1316	0.3193
13.	<i>TRI</i>	14.636	0.0699
14.	<i>SB</i>	<i>infinity</i>	<i>infinity</i>
15.	<i>SPI</i>	<i>infinity</i>	<i>infinity</i>
16.	AP	1.9128	0.5228

702
703
704**Table 10b**
MC statistics (T and VIF) used for the modelling

S/NO	Criteria	VIF (< 10)	T (> 0.1)
1.	NDVI	2.1910	0.4564
2.	GY	2.2275	0.4489
3.	LD	1.5132	0.6608
4.	RD	6.6860	0.1496
5.	PSW	2.2299	0.4485
6.	SP	1.6540	0.6046
7.	DD	2.6276	0.3806
8.	TWI	3.1316	0.3193
9.	AP	1.9128	0.5228

705
706
707
708
709
710

land use/land cover (LL), normalized difference vegetation index (NDVI), geology (GY), **soil type (ST)**, lineament density (LD), rainfall distribution (RD), proximity to surface water bodies (PSW), slope (SP), **geomorphology (GM)**, drainage density (DD), **elevation (EL)**, topographic wetness index (TWI) Topography **ruggedness index (TRI)**, **soil permeability (SB)**, **stream power index (SPI)**, and aspect (AP).

711
712
713
714
715
716
717
718
719
720

4.2. Sensitivity analysis

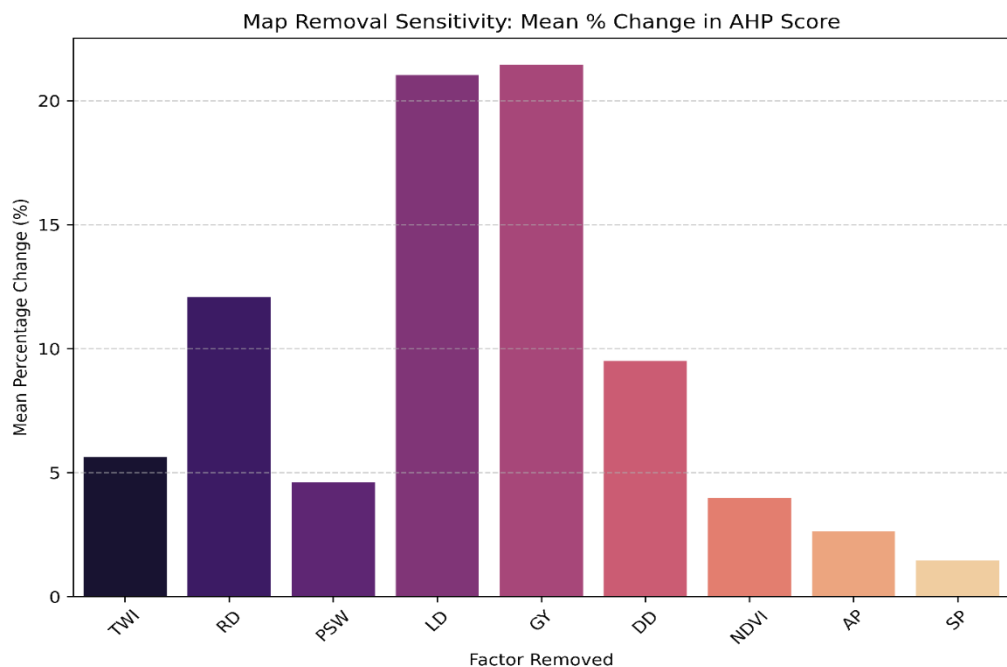
In an MCDA, sensitivity analysis is required to ensure that the result is dependable notwithstanding the variable nature of expert assessments. **Table 11** summarizes the overall implication of each theme layer to the GWP zone modelling map. Regardless of the variations in mean percentage change (MPC), removing a thematic layer has a substantial effect on the final map. Thus, each determining component included in AHP analysis has a unique function in defining the GWP zones. In this analysis, the most significant sensitivity index is obtained by deleting the geological layer with the highest comparative score of 21.45%. Furthermore, groundwater is slightly susceptible to LD, LD, DD, TWI, PSW, NDVI, AP, and SP, with MPC values of 21.045, 12.083, 9.5126, 5.6305, 4.6139, 3.9813, 2.6305, and 1.4579%, respectively (**Fig. 4**).

721
722**Table 11**
Statistical study of map removal SA.

S/NO.	Removed Factor	Mean Abs. Change	Max. Abs. change	Min. Abs. change	Std. Abs. change	Mean %_change
1.	NDVI	0.0172	0.0816	0.0000	0.0147	5.6305
2.	GY	0.0358	0.1225	0.0000	0.0293	12.0830
3.	LD	0.0137	0.0513	0.0000	0.0101	4.6139
4.	RD	0.0647	0.1467	0.0021	0.0286	21.0451
5.	PSW	0.0639	0.1845	0.0000	0.0420	21.4592
6.	SP	0.0254	0.0825	0.0003	0.0187	9.5126
7.	DD	0.0110	0.0332	0.0001	0.0086	3.9813
8.	TWI	0.0069	0.0205	0.0000	0.0050	2.6305
9.	AP	0.0045	0.0163	0.0001	0.0031	1.4579

723

724



725

726 Fig. 4: A bar graph illustrating the mean percentage of the map removal analysis's AHP score

727 4.3. Analysis of thematic layers

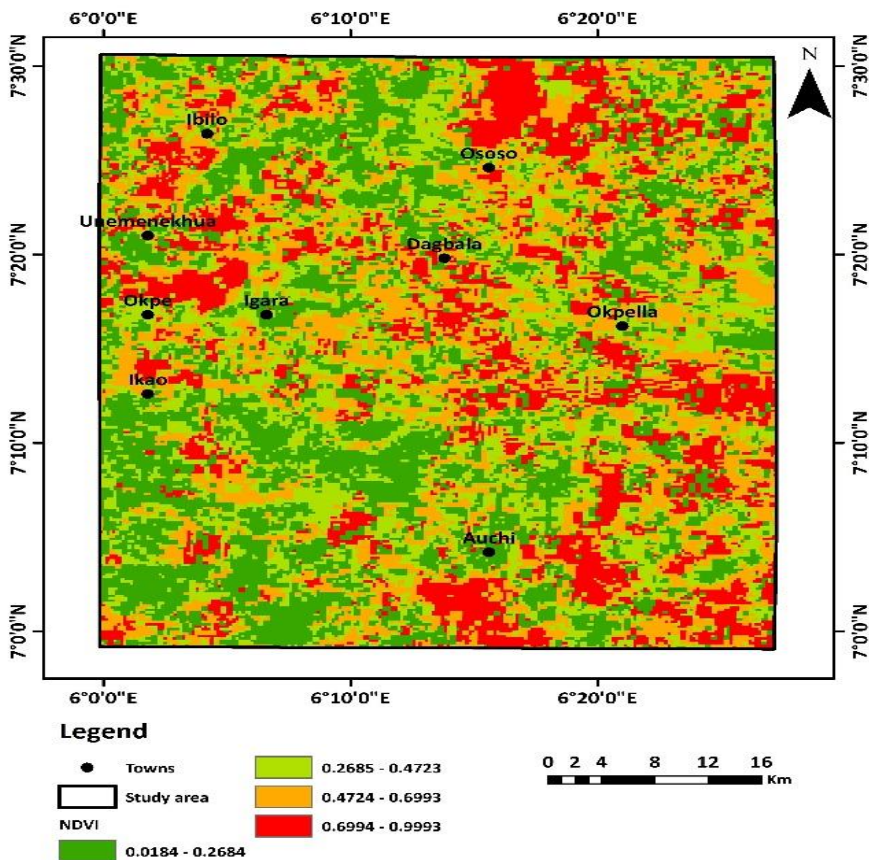
728 In general, GW production for a given aquifer is determined by a number of factors, including anthropology,
729 hydrogeology, hydrology, and topography, all of which are dependent on data that is readily available and of good
730 quality. RS data are often large in size and contain detailed geographical information. The following
731 characteristics provide a quick overview of the theme layers employed in the study.

732 4.3.1. Anthropological (NDVI) characteristics and groundwater potential

733 **NDVI:** The NDVI is a useful metric for measuring vegetative component activity in ecosystem patterns, while
734 the productiveness of vegetative coverings pertains to water loss and precipitation (e.g., Hussain et al., 2022;
735 Ozegin and Ilugbo, 2025). It is a broadly utilized measurement that monitors changing vegetation on both a global
736 and regional basis. Consequently, it has profound effects with regard to groundwater accumulation and
737 accessibility. Tucker (1979) developed this metric, which spans from -1 to 1. Numbers below 0 indicate no
738 vegetative cover, while values above 0 indicate accessible cover. In this study, areas' NDVI was classified into
739 four groups using thematic mapping: 0.0184-0.02684, occupying 32%; 0.02685-0.4723, occupying 25%; 0.4724-
740 0.6993, occupying 25%; and 0.6994-0.9993, occupying 18% (**Fig. 5** and **Table 5**). An abundance of flourishing
741 greenery in a specific location emerges to be strongly associated with optimal groundwater recharge—vegetation
742 designations range from 0.2 to +1 (Goward et al., 1991; Ozegin and Ilugbo, 2025). Consequently, the higher the
743 score, the more significance is assigned, while minimal vegetation and grasses receive only a small percentage of
744 weight. A greater NDVI implies extensive vegetation cover, given vegetation decreases runoff (e.g., rainwater)
745 and helps to recharge groundwater reservoirs (Hasanuzzaman et al. 2022). The volume of precipitation,
746 temperature, soil utilization, vegetation moisture content, soil moisture, and evaporation are all controlled by
747 groundwater depth.

748

749



750

751 **Fig. 5.** Anthropological factor—normalized difference vegetation index

752

753 **4.3.2. Hydrogeological (LD and GY) characteristics and groundwater potential**

754

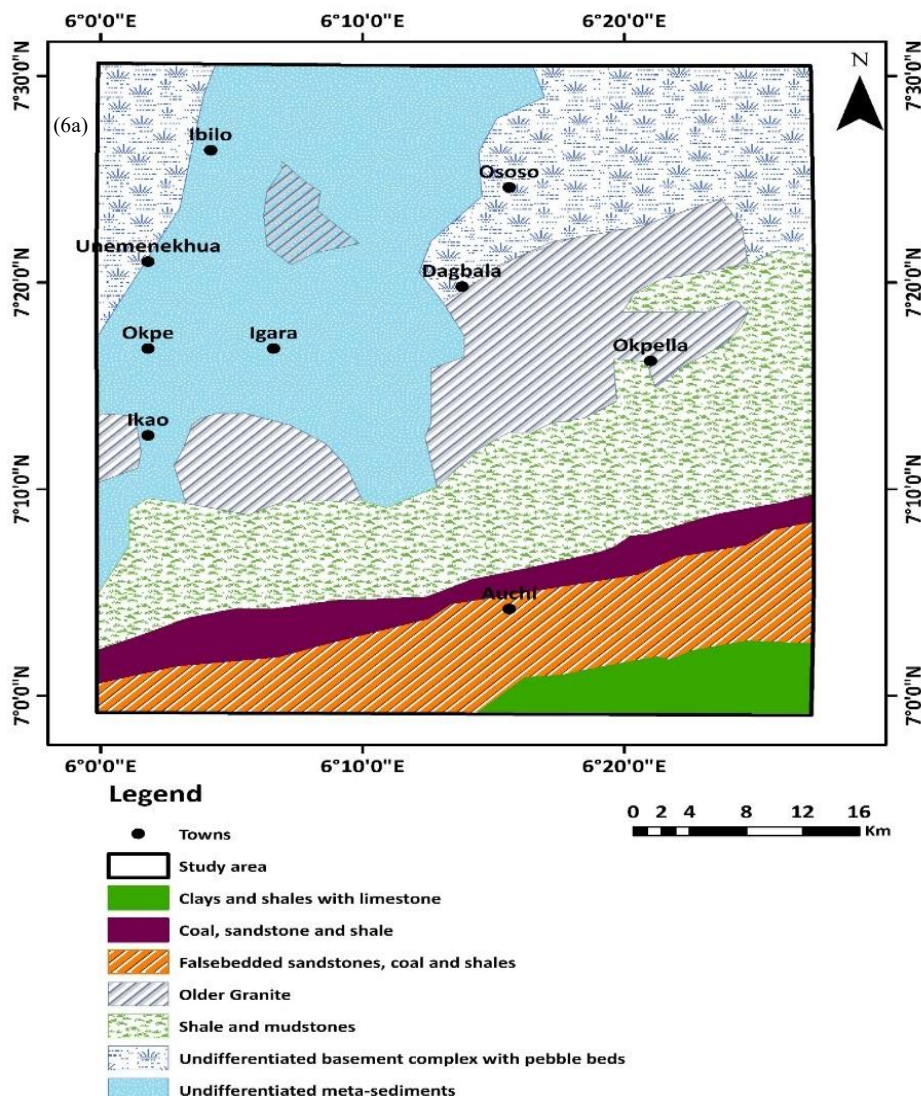
755 **LD:** Any linear geological characteristic, including faults and fractures, that develops from the pressing and
 756 shearing forces connecting geologic formations is called a lineament. It is a geological framework that can be
 757 used as an effective guide when studying the hydrogeology of a basement. As a result, lineaments are capable of
 758 showing surface structure, including fractures, fissures, and defects, among others. The arrangement of structural
 759 elements that produce secondary porosity in the rocks determines hydrogeological processes and the presence of
 760 groundwater in the rocky landscape (e.g., Al-Djazouli et al., 2020). Lineaments affect subsurface passage of water
 761 and spread to optimize flowing paths. Groundwater activity can be better understood by methodically examining
 762 the concentration, direction, and intersection patterns within lineaments (e.g., Ilugbo et al., 2023a, b).

763 The lineament map for the investigation region is shown in **Fig. 6a**. The northern section of this research region
 764 is notable for fairly substantial lineament density. Higher lineament densities are indicative of optimized porosity,
 765 facilitating groundwater supplies. Areas with a substantial lineament density are considered to have good
 766 prospects for groundwater and receive a greater ranking based on good pore size and permeation, while areas with
 767 low to moderate lineament density are considered to have poor groundwater possibilities and are given lower
 768 rankings.

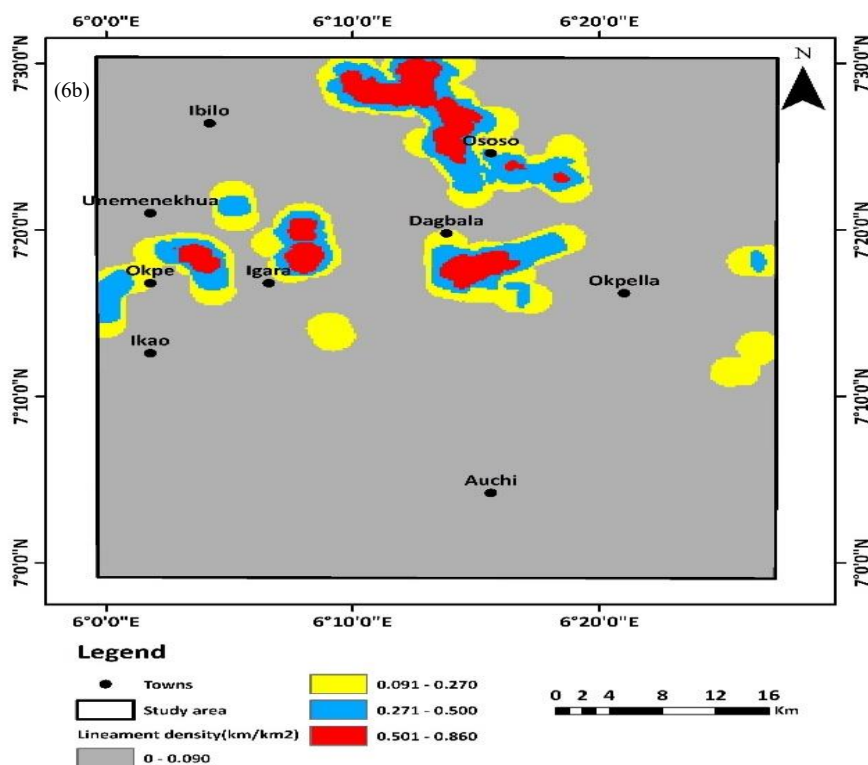
769

770 **GY:** Geology constitutes one of the most important hydrogeological criteria since it indicates the structural
 771 characteristics of the geographic rocks that shape the accumulation of groundwater. The properties of the major
 772 lithological development in the geographic region worthwhile have a significant impact on the pattern of
 773 distribution, happenstance, and condition of groundwater. GY completely controls groundwater migration and
 774 absorption since the number of pores and permeability in aquifer rocks are inherent features (Ilugbo et al., 2023b).
 775 The hydraulic conductivity within a lithologic structure or its weathered consequence increases the pace of water
 776 penetration and flow through it, as well as its capacity for storing underground water (e.g., Rajendran et al., 2020).

777 The explored location's groundwater availability is largely determined by the hydraulic characteristics of the
 778 crystalline basement rocks; therefore, older granites are capable of simply behaving as groundwater storage
 779 facilities when they are weakened and/or fragmented.
 780 In this study, geological structures have changed from the undifferentiated basement complex and undifferentiated
 781 meta-sediments in the northern section of this research location, whose components are interspersed with granite
 782 gneiss, shale, and mudstones (**Fig. 6b**), to the distinguishing sedimentary composition formation in the southern
 783 part, which is composed primarily of clays and shales alongside limestone, coal, sandstone, and shale; false-
 784 bedded sandstones; coal; and shales. The mild slope decreases in the direction of the southern regions of the
 785 research zone, and the deposition of the basement rocks found in the northern mountainous terrain could
 786 potentially be the cause of the phenomenon. The research area's lithologic components were classified as 1 (false-
 787 bedded sandstone, coal, and shale), 2 (coal, sandstone, and shale), 3 (clays, shales with limestone, Older granite,
 788 and undifferentiated basement with complex pebbles), and 4 (shale and mudstones and undifferentiated meta-
 789 sediments), which indicate very low, low, moderate, and high groundwater potentialities, respectively (**Table 5**).
 790 These covered 505 km² (21%), 529 km² (22%), 739 km² (21%), and 265 km² (11%), respectively. The lithology
 791 rated 3 and 4 has substantial consequences on groundwater spread and accessibility (Rahmati et al., 2016; Ozegin
 792 et al., 2023; 2024b). Every lithologic category was assigned a weight based on its relevance for groundwater
 793 availability and hydrodynamic qualities. Groundwater phenomena are determined by the interwoven interplay of
 794 lithological properties, usage of land, terrain, and watershed environment.
 795



796



800 Fig. 6. Hydrogeological factors—a. lineament density and b. geology

801 4.3.3. *Hydrological (RD and PSW) characteristics and groundwater potential*

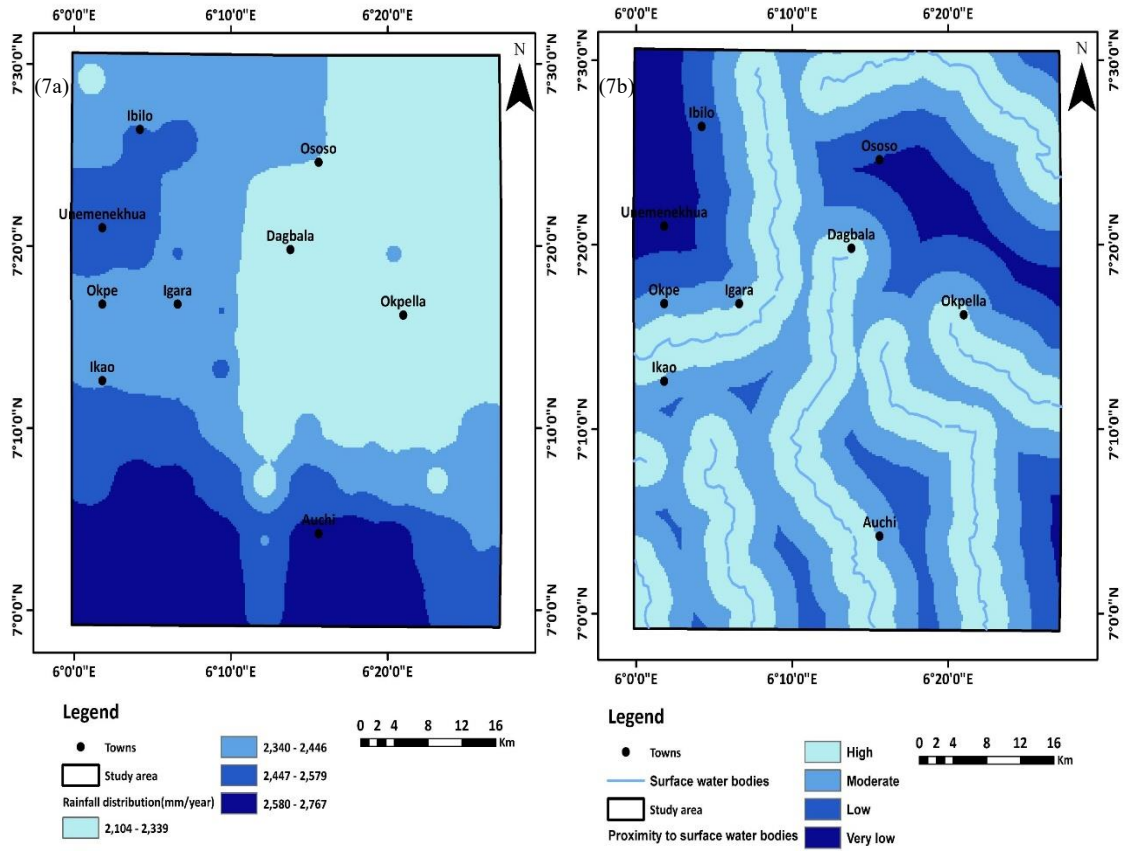
802 **RD:** The hydrology and hydrogeological functions of an area are greatly influenced by both the spatial and time
 803 course of rainfall (Ozegin et al., 2024a, b). It is the main and potentially important mechanism of groundwater
 804 restoration. With yearly projections varying from 2,104 mm to 2,767 mm, rainfall is the primary contributor to
 805 groundwater replenishment in the research location (Fig. 7a). The research region is separated into four rainy
 806 categories based on the amount of rainfall obtained: 34% of the total area is classified as very low, 32% as low,
 807 17% as moderate, and 17% as high (Table 5). The amount, length, and extent of rainwater all affect the pace of
 808 penetration and subsequent discharge. Low absorption and high surface discharge are impacted by prolonged low
 809 precipitation. The annual mean rainfall has an impact on groundwater recharge as well. While less precipitation
 810 indicates a low groundwater possibility, more rainfall indicates higher groundwater prospects. There were
 811 considerable amounts of rain in the southwest area. When defining groundwater zones, heavier precipitation zones
 812 are given more weight, and vice versa.

813

814 **PSW:** Groundwater replenishment processes are directly impacted by how far it is to surface bodies of water,
 815 which indicates the nearness of every location in the research region to the closest body of water (e.g., Arabameri
 816 et al. 2021; Ozegin et al., 2024a). It is an essential variable in the mechanisms of surface-groundwater and aquifer
 817 recharge prospects. Those for influent flow facilitate groundwater runoff, while those for effluent flow maximize
 818 groundwater recharging. When compared with places more remote, groundwater potential is typically higher near
 819 water sources (rivers or streams) because they serve as a source of a refill for the nearby aquifers, especially during
 820 times of excessive flow (e.g., Maity and Mandal, 2019; Naghibi et al., 2020; Mathewos et al., 2024). As a result,
 821 groundwater prospect delineation is correlated with the proximity to water bodies.

822 The buffered areas nearest to water bodies received the maximum score of 4, while those situated most remotely
 823 received a lesser score of 1, signifying the greatest and smallest prospects for replenishment of groundwater,
 824 respectively (Table 5). The flow condition in the research area can be regarded as effluent. The buffer regions are
 825 categorized into four categories: "high (888 km), moderate (872 km), low (330 km), and very low (300 km)" (Fig.

826 7b). Inevitably, when proximity to water bodies (such as streams) decreases, the weight value rises, indicating
 827 enhanced groundwater possibilities (e.g., Arabameri et al., 2021; Ozegin et al., 2024a).



828
 829 **Fig. 7.** Hydrological factors—*a.* rainfall distribution and *b.* proximity to surface water bodies

830 *4.3.4. Topographical factors (SP, GM, DD, TWI, and AP) characteristics and groundwater potential*

831 **SP:** Typically, SP specifies the vertical extent of every geologic framework across the earth and consequently
 832 plays a decisive role in influencing the gravity-driven passage of water (Chen et al., 2019; Shahinuzzaman et al.,
 833 2021; Ilugbo et al., 2023). It provides vital information about regionally focused geologic and geodynamic
 834 phenomena. The SP of an area, usually determined by elevation, entails the sharp descent from a lateral surface.
 835 Slope influences the passage of water based on gravitational pull, revealing the speed of subterranean longitudinal
 836 transmittance. As the SP rises, the water makeup of the soil becomes exceedingly hard to maintain, as water runs
 837 off faster and gets less soaked by the earth's pores.

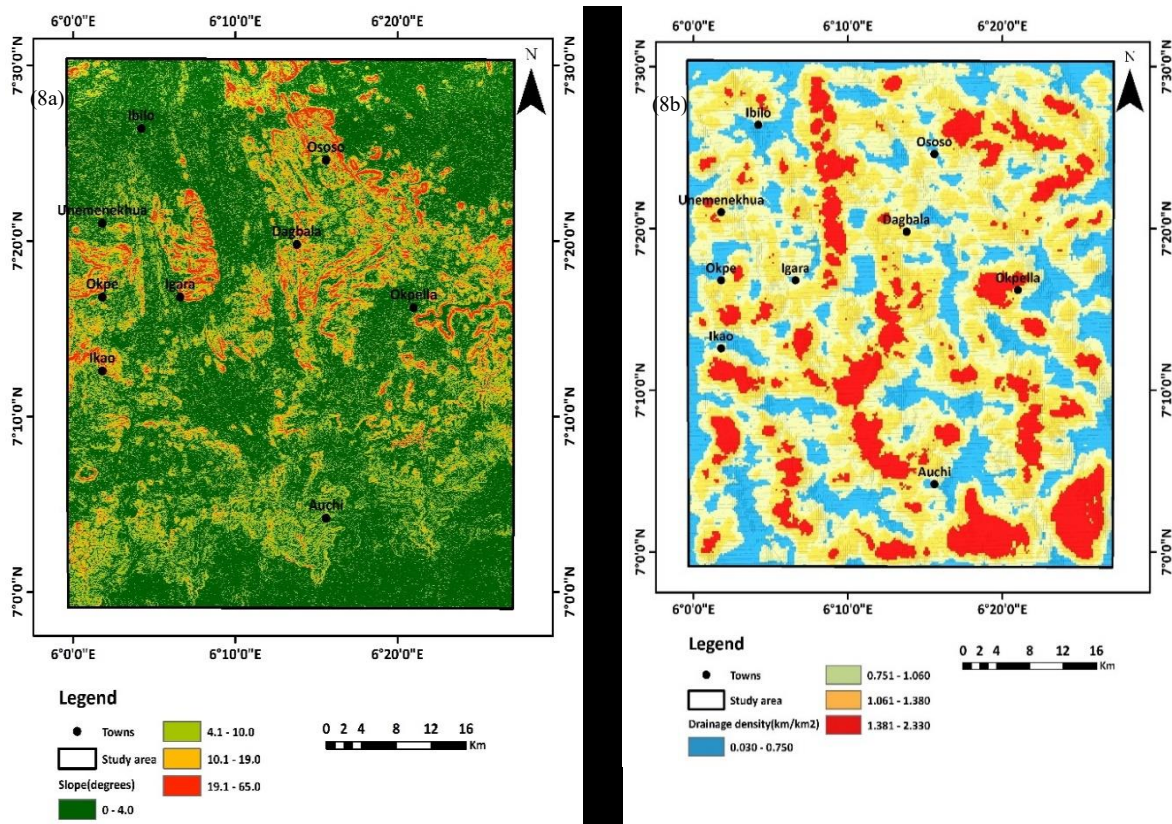
838 During a rain, rainwater rapidly sweeps along steep slopes, resulting in reduced recharge at greater slope
 839 inclinations. The research area map's slope is displayed in **Fig. 8a**. Four categories—very low (19.1–65.0°), low
 840 (10.1–19.0°), moderate (4.1–10.0°), and high (0–4.0°)—were created from the reclassification of the slope values.
 841 A more significant weight is assigned to mild and even slopes, while less weight is assigned to steep and
 842 exceedingly steep slopes (**Table 5**). 25% (minimum area) of the study region consists principally of 0–4.0° values
 843 rated high (4). Consequently, the minimal area has a level slope that retains groundwater. The aquifer recharging
 844 decreases as the slope gets steeper. It occurs because rainfall creates an intense rush of water downward on the
 845 steep gradient, resulting in minimal absorption. Table 5 shows that slope inclination is inversely correlated to
 846 surface runoff permeation (Wang et al., 2018; Morbidelli et al., 2018; Ozegin and Ilugbo, 2024; Zheng et al.,
 847 2024).

848 **DD:** Drainage density, which represents the number of networks moving surface water, is regarded as one of the
 849 primary signals of potential groundwater reserves in a given location. DD increases groundwater outflow while
 850 lowering recharge potentials. As a result, land with a compact watercourse exhibits a rapid recharge rate, but the
 851 contrary is similarly applicable (Roy et al., 2019). Four drainage densities were identified for the groundwater

852 potential in the research region based on the drainage map (**Fig. 8b**): high (0.0300-0.750 km/km²), moderate
853 (0.751-1.060 km/km²), low (1.061-1.380 km/km²), and extremely low (1.381-2.330 km/km²). 1,261 km² (53%) of
854 the research region had high and moderately substantial groundwater prospects (**Table 5**). The DD of the
855 hydrographic arrangement indicates various physical conditions, including the proportion of surface and
856 subsurface movements. This threshold, which favours slope drainage, allows us to appreciate the significance of
857 surface drainage. This signifies the water-striking system's mean length per kilometre. Thus, increased DD
858 reduces the likelihood of absorption and recharging of groundwater. Determinants like geology, penetration,
859 runoff, waters, plant diversity, and climate have an immediate effect on DD (e.g., Al-Djazouli et al., 2020).

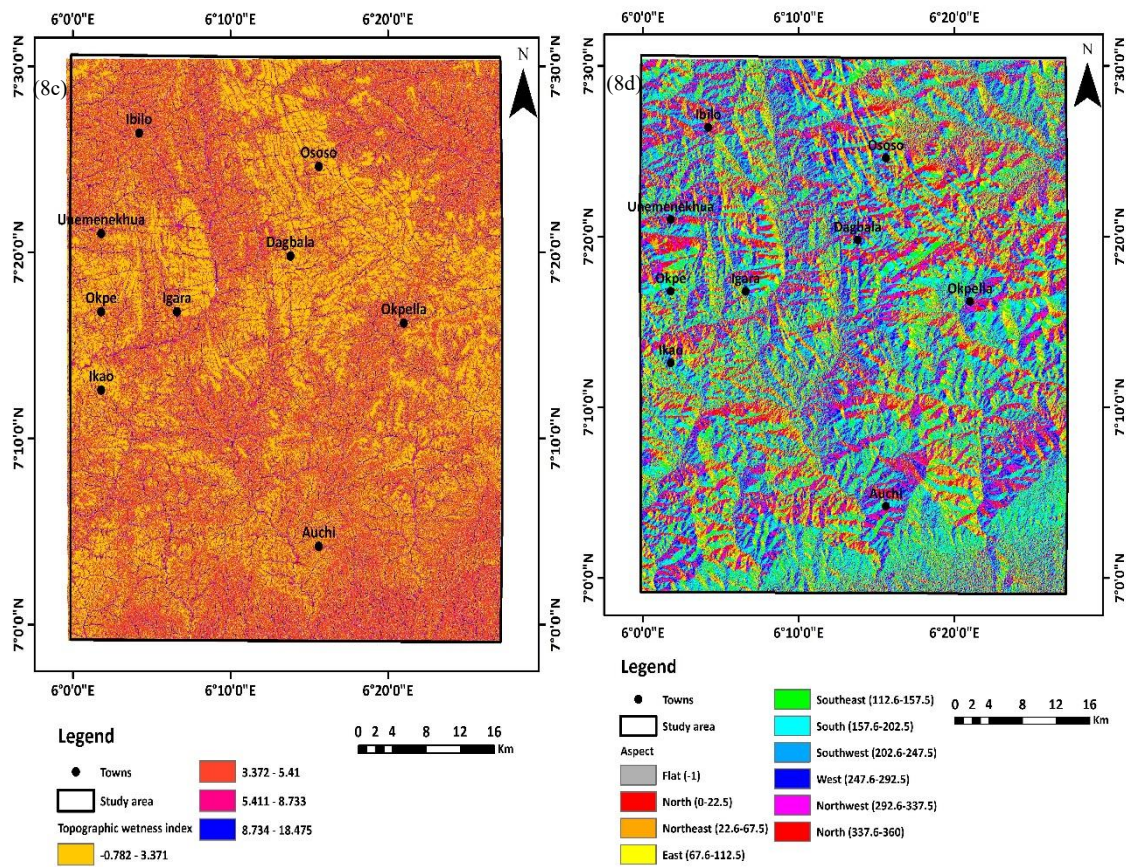
860 **TWI:** The TWI is a frequently used metric to assess the influence of geographical features on watershed dynamics
861 (Sørensen et al., 2006; Ozegin and Ilugbo, 2025). It is an indicator that describes the amount of hydration or
862 saturated states in a given region. In the course of an intense downpour occurrence, areas exhibiting high TWI
863 values retain greater amounts of water than other areas, resulting in a saturated state (Ozegin and Ilugbo, 2025).
864 **Fig. 8c** depicts the TWI map for the study region, which gives an illustration of the geographical spread of TWI
865 values and the consequences for GWP across the entire study area. Recognizing that hillslope impact, the TWI
866 aids in finding locations with characteristics that are more probable to create floods than to encourage
867 replenishment of groundwater. Low (-0.782 and 3.371), moderate (3.372 and 4.410), high (4.411 and 8.733), and
868 very high (8.733 and 18.475) constitute the four categories into which the TWI metrics in this research are
869 reclassified. Lower weighting is assigned to locations with lower TWI ratings in the distribution of GWP,
870 indicating a limited capability for groundwater recharging. Locations that have larger TWI values, which indicate
871 suitable replenishment conditions, are given greater significance (e.g., Zhao et al., 2024). This metric takes into
872 account simultaneously the inclination and the upstream influencing location per unit width perpendicular to the
873 course orientation. It provides useful details about the hydrology dynamics in a given locale. There exists a
874 positive correlation since the highest TWI value indicates a high subsurface water prospect and vice versa.
875

876 **AP:** Aspect is the slope's foremost orientation and defines the perspective of the watercourse (Razavi-Termeh et
877 al., 2019). This regulates slope development, including lineament, precipitation, wind consequences, and direct
878 sunlight (Solomon and Quiel, 2006; Zabihi et al., 2016). It is commonly employed in mountainous and rugged
879 places, considering the period of sunlight or obscurity has an important influence in determining soil wetness
880 (Sinha et al., 2012). The aspect additionally influences the formation of runoff through the development of
881 vegetation and GW enhancement (Ahmed and Sajjad, 2018). This component is categorized into ten groups, as
882 shown in **Fig. 8d**. Evidently, the area of a shady slope with significant soil humidity has an abundance of flow.
883 For flat-facing sides to the north, northeast, northwest, and north, aspect-influencing feature classifications are
884 predominant, suggesting a high probability of groundwater prospects. Conversely, the other aspect classes have
885 the lowest scores (**Table 5**), which suggests that there is minimal likelihood of groundwater prospects.
886



887

888



889

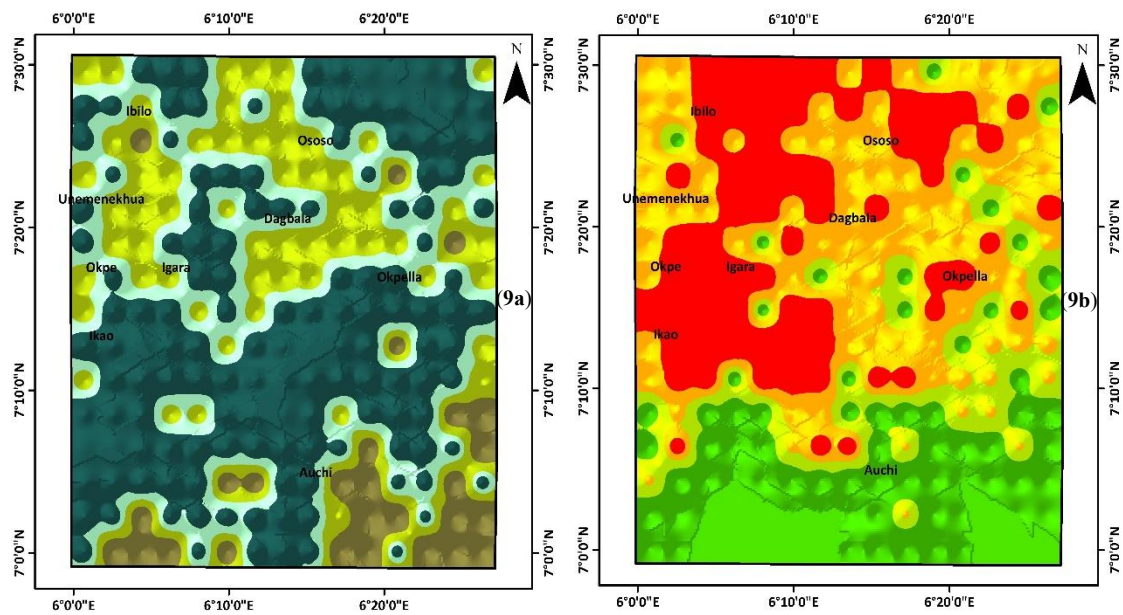
890 **Fig. 8.** Topographical factors—a. slope; b. drainage density; d. aspect; and e. topographic wetness index

891 4.4. GW potentiality modelling

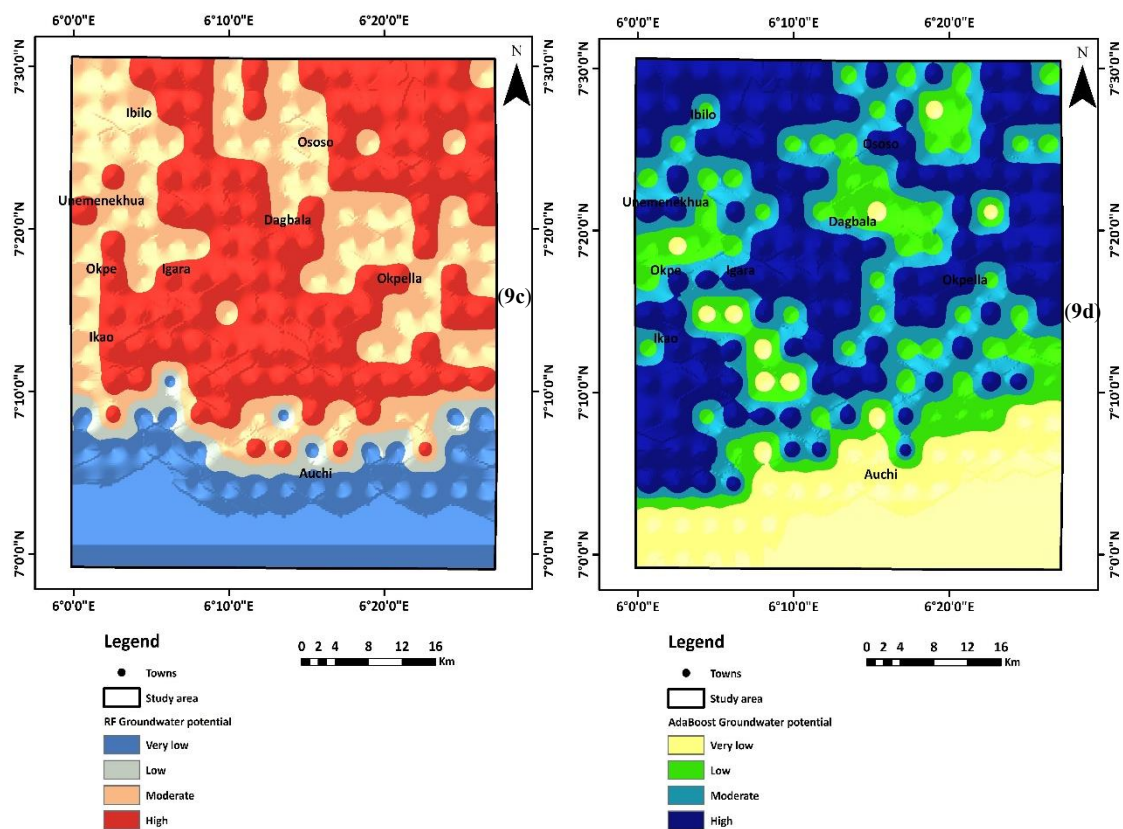
892 Long-term development requires proper GWP zone characterization. Given that groundwater is an inherent asset,
893 its amount has been decreasing due to a variety of anthropological and natural phenomena. Groundwater
894 management plays a critical role in regional planning and long-term sustainability. As an effect, the GWP zones
895 in the study area have been established based on the research data. This work prioritizes projecting GWP zones
896 using AHP-based MCDA, and ML approaches include AdaBoost, RF, SVM, and XGB. These methods were used
897 to examine groundwater geoenvironmental factors, which included topographical, hydrological, geological, and
898 anthropogenic features critical for determining groundwater distribution. **Fig. 9** depicts the geographical spread
899 of GWP zones calculated using AHP-based MCDA and four contemporary ML algorithms: AdaBoost, RF, SVM,
900 and XGB. "Jenks' natural breaks classifier" in a GIS context was leveraged to classify each of the GWP maps
901 into four categories (high, moderate, low, and extremely low). A greater GWPZ rating implies a significant
902 quantity of groundwater potential, whereas a lower GWPZ index figure suggests a smaller quantity of water
903 beneath the ground surface.

904 The AHP model demonstrates exclusively that 14.03% of the entire watershed area has "high" groundwater
905 potential, with a further 32.30% rated to exhibit "moderate" potential. The GWP zone ratings, attributed to the
906 Random Forest results, indicate areas covered of 23.50, 4.00, 30.83, and 41.59% for very low, low, moderate, and
907 high potential, respectively. According to the SVM model, there is "high" groundwater potential in 45.93% of the
908 basin's total area and "moderate" potential in a further 21.54%. Based on the AdaBoost model, 36.42% of the
909 study's entirety has "high" groundwater potential, and a further 23.29% has "moderate" potential. In contrast,
910 59.23% of the area coverage in the XGB model is made up of the high and moderate potential categories (**Fig.**
911 **10**). For GWP zones with descending high prospect values, the SVM, RF, AdaBoost, XGB, and AHP modes
912 generally show a spatial extent of 45.93, 41.59, 36.42, 25.30, and 14.03%, respectively. Moreover, it is evident
913 that there is considerable potential for underground water in parts of the study location with high rainfall,
914 lineament density values, and maximum geology rating. On the other hand, high slope and PSB values are
915 indicative of regions with very low to low groundwater potential. According to the models (e.g., SVM, RF, and
916 AdaBoost), the northern portion of the research zone has a larger potential for GW and should be explored for
917 GW development. Conversely, the study demonstrates that the southern section of the research area has low GW
918 potential, which is attributed to longer distances to wetlands and lower lineament density. The SVM model
919 estimates that the high GWP zone occupies approximately 1098 km², or 45.93% of the overall research area (**Fig.**
920 **10** and **Table 12**). The existence of high lineament density indicates that there is substantial hydro-potential
921 development; however, the entire lineament density in the evaluated terrain is low (Ozegin et al., 2023). Research
922 indicates that diverse morphologies on earth's surface led to distinct types of freshwater accumulation (Rajaveni
923 et al., 2017; Prasad et al., 2020). The differences in the availability of GWP zones resulting from the modelling
924 approaches are highlighted by the geographical contrast shown in **Figs. 9a-e**. SVM and RF performed better than
925 other models in establishing GWP zones, which can be utilized to evaluate regulating land use and water supply.
926 The combination of powerful ML algorithms and AHP with an extensive repertoire of contextual variables
927 resulted in nuanced and remarkably accurate approaches to estimating GW potential zones in the research area.
928 The aforementioned technique can considerably improve long-lasting GW planning and oversight. The various
929 influencing features gave an in-depth understanding of the groundwater context, including both natural and
930 human-induced aspects. The study highlights the effectiveness of ML approaches in environmental and
931 governance of resources, laying the groundwork for subsequent studies in related areas. Prospective studies might
932 extend the framework by including contemporaneous data and variable land-use patterns to improve the models'
933 predictability and application for effective watershed management.

934
935
936



937



938
939

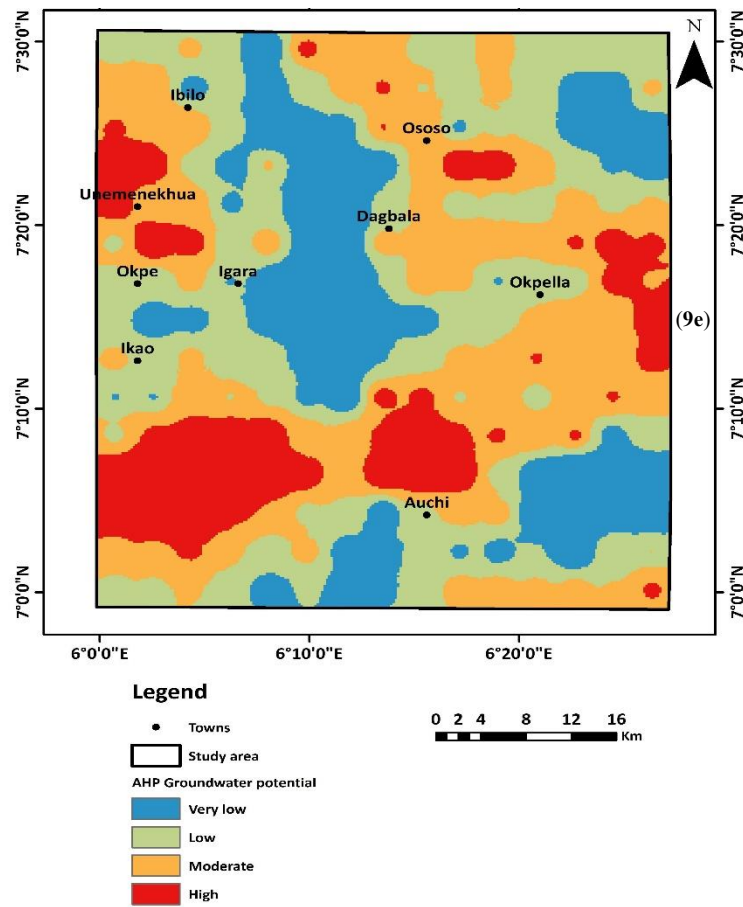


Fig. 9. GWP zone: a. SVM b. XGB c. RF d. AdaBoost, and e. AHP

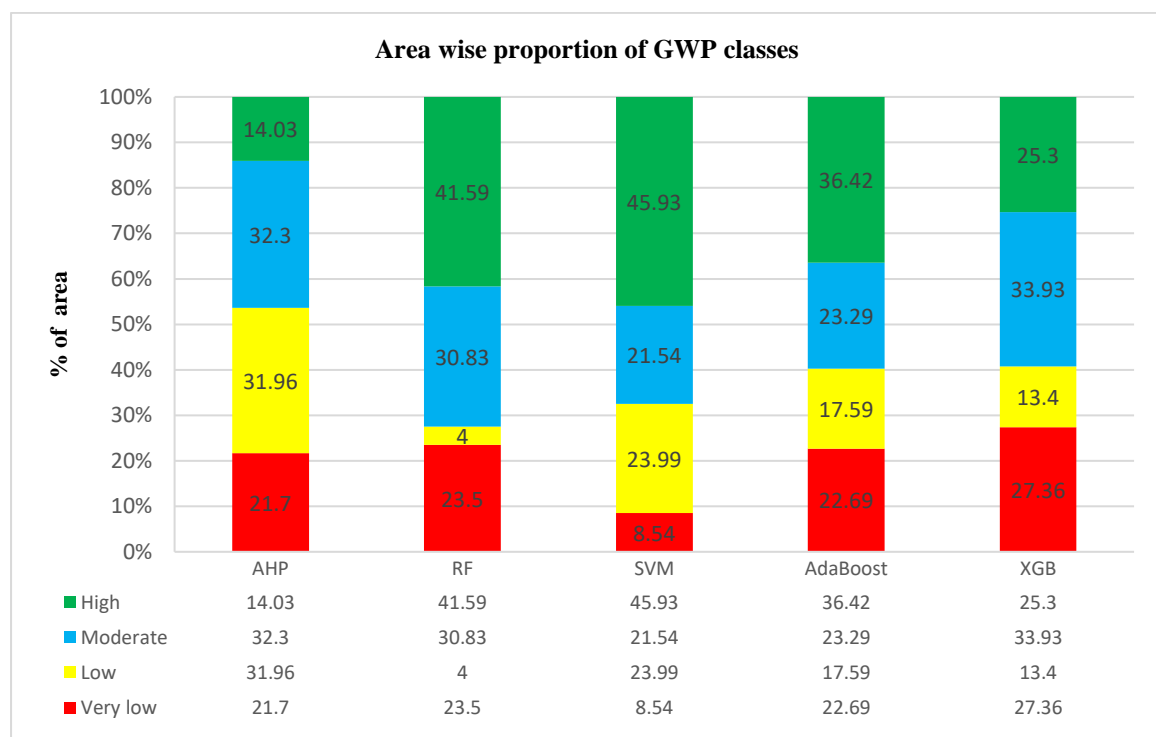


Fig. 10. Area-wise component of GWP classification: AHP, RF, SVM, AdaBoost, and XGB

947 **Table 12.**

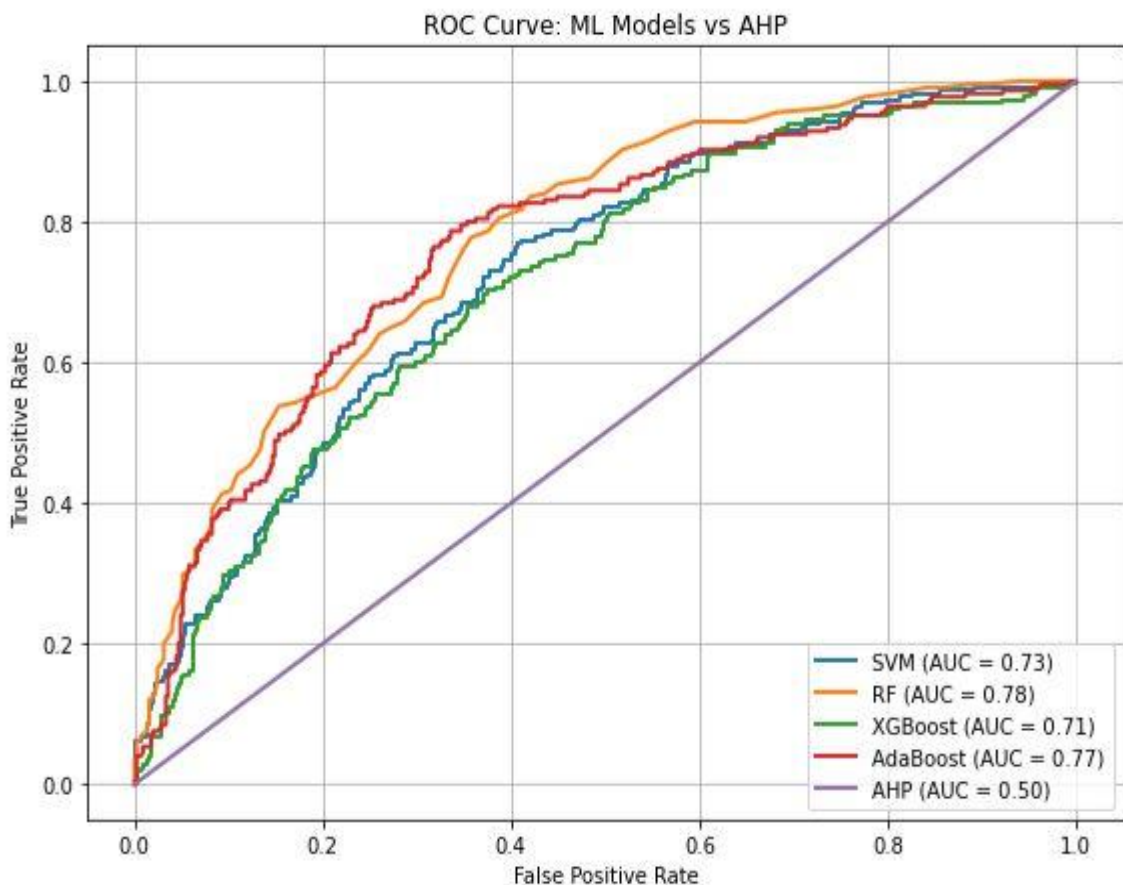
948 Area under GWP zones of distinct models in square kilometres and percentages

GWP class	AHP (km ²)	AHP (%)	RF (km ²)	RF (%)	SVM (km ²)	SVM (%)	AdaBoost (km ²)	AdaBoost (%)	XGB (km ²)	XGB (%)
Very low	519.00	21.70	562.00	23.50	204.00	8.54	542.00	22.69	654.00	27.36
Low	764.00	31.96	96.00	4.00	573.00	23.99	420.00	17.59	320.00	13.40
Moderate	772.00	32.30	737.00	30.83	515.00	21.54	557.00	23.29	811.00	33.93
High	335.00	14.03	994.00	41.59	1098.00	45.93	871.00	36.42	605.00	25.30

949

950 4.5. Evaluation of models and contrasting the suitable frameworks

951 The ROC curve is an effective approach for evaluating the categorical outcome of AHP and ML models. It gives
 952 information on a model's ability to distinguish between instances that are positive and negative. The AU-ROC
 953 indicator measures a model's general success, with a greater AUC value indicating better predictive capacity. The
 954 AUC scores for the ML models and AHP are shown subsequently (**Fig. 11**): RF had an optimal AUC of 0.78,
 955 preceded by AdaBoost (0.77), SVM (0.73), XGB (0.71), and AHP (0.50). These AUC values indicate the models'
 956 capacity to distinguish between prospects for GW and non-prospect areas. The study of the ROC curve yielded
 957 an AUC value of 0.78 to 71 for ML, suggesting a good outcome because it fits within the spectrum of 0.71-0.80,
 958 as shown in **Fig. 11**. As a result, the use of ML algorithms in this work produced adequate spatial predictions of
 959 groundwater potential. Conversely, AHP ranges from 0.50 to 0.60, indicating minimal efficiency. Prior studies
 960 (e.g., Masroor et al., 2023; Ali et al., 2023; Ozegin et al., 2024b; Sharma et al., 2024) have also used the AUC
 961 values from the ROC curve to assess the exactitude of the created GW prospective zone.



962

963 **Fig. 11.** ROC curve-based prospect appraisal for a GW map.

964

965

966 4.6. Limitations
967 Certain limitations must be taken into consideration, even if the study uses a scientific method that is budget-
968 friendly for analyzing different geoenvironmental criteria. The following defines the primary constraints:
969 The multifaceted geological nature of the subject areas is an important bottleneck to this research. The variability
970 caused by different rock categories, geologic frameworks, and features, including folding and fractures, makes it
971 difficult to determine GWP zones. This research's satellite and field information are heavily reliant on satellites
972 provided by a variety of categories (e.g., agencies). Even so, the map's greatest strength is its incredibly extensive
973 regional coverage. A significant variation in all of these factors can be found at small scales. As a result of this
974 issue, the resulting GWP mapping could prove inaccurate on the local level. There are some limitations associated
975 with predicting groundwater modelling. These are often related to inadequate quantity and quality of data, as well
976 as mistakes in the model's intrinsic configuration and designations. Considering this study, having 36 ground-truth
977 indications, an implication of sample size was incapable of being eliminated under this threshold. A detailed choice
978 of attributes and adjustments can assist in improving prediction power by reducing potential constraints.
979 One limitation is that fishnets impose an artificial grid structure that may not align perfectly with the actual
980 geographic patterns. Also, the cell size can drastically impact the analysis results. Choosing an appropriate cell
981 size is a key factor in effective analysis.

982
983 4.7. Interrogating the potential impacts of the SDGs

984 Lack of data and monitoring limitations continually inhibit precise evaluation of the remaining SDG 6 targets,
985 which include managing water resources, water quality, aquatic ecosystems, and a supportive environment. To
986 attain the SDGs, it is critical to highlight the significance of this study within the overall framework of a
987 sustainability strategy, notably within the framework of managing water resources. The SDGs represent an
988 extensive ensemble of global initiatives aimed at ensuring a sustainable future for human civilization. This entails
989 a wide range of the financial, ecological, and interpersonal phenomena. In the setting of this current study, using
990 the ML and AHP models to identify the prospect for GW zones would provide reliable data on the state of
991 groundwater that eventually contributes to the achievement of SDG Goal 6 (clean water and sanitation). Besides,
992 the accurate and reliable outcomes of the ML-based GIS model in locating appropriate agriculturally championed
993 GW resources will strengthen its long-term viability to aid in the achievement of the Sustainable Development
994 Goals: zero hunger (Goal 2) and good health and well-being (Goal 3) through sustainable management of
995 terrestrial ecosystems and their services (SDG 15) and mitigating the effects of climate change (SDG 13). Thereby
996 strengthening sustainable water, food, and energy nexuses and fostering perspectives for a reliable water future.

997 5. Conclusion

998 Defining appropriate areas for GWP is critical to ensuring the effective and long-lasting utilization of existing
999 water assets in the research area. In locations where data is limited, RS-based data sources can give insightful
1000 knowledge. AHP, SVM, XGB, RF, and AdaBoost were employed in this work. Nine thematic maps (normalized
1001 difference vegetation index, geology, lineament density, rainfall distribution, proximity to surface water bodies,
1002 slope, aspect, drainage density, and topographic wetness index) were developed with an impact on regional
1003 groundwater. The study area is characterized by a wetland environment, a minimal number of lineaments, a
1004 progressive slope, and homogeneous alluvial deposit geology; every one of these factors influences GW. Based
1005 on the greater density of lineaments, the precipitous slope, and the availability of geological features, the
1006 northeastern portion of the study region presents certain challenges. Geology, rainfall, and lineament density had
1007 the largest impact on GWP zone delineation throughout the entire model. Four plausible zones are highlighted on
1008 the GWP zone map created by ArcGIS spatial analysis tools: "very low, low, moderate, and high." Wetlands and
1009 agriculture-related areas have a high and moderate GWP zone. Every model, consisting of AHP, SVM, XGB, RF,
1010 and AdaBoost, identifies high GWP zones within the range of 14.03-45.93% of the overall area, while very low
1011 groundwater potential zones cover 8.54-27.36%. The effectiveness of the model was verified using ROC to
1012 corroborate the GWP zones. The findings show that RF and AdaBoost surpass GWP zone estimation. The
1013 outcomes of verification considerably improve the dependability of the methods used. These frameworks will be
1014 beneficial for effectively assessing groundwater replenishment and directing the best place for artificially
1015 constructed replenishing mechanisms and other watershed planning projects. The approaches used in this study,

which is based on conceptualization needs and is systematic in nature, can be easily employed everywhere data is available, independent of the alterations needed to tackle concerns such as water scarcity and changing climates. The GW recharging prospect map serves as an archive for resource knowledge, which may be updated on a regular basis by combining fresh data and other thematic map kinds. The study demonstrates dependable modelling of GW prospects gets established by combining remotely observed features, groundwater bore data, and themed data. Furthermore, the study improves our comprehension of major discoveries identified during expeditions with local populations. However, the widespread harvesting of groundwater for use in factories using deep-water motors, especially during the warmer seasons of November to February, offers a serious challenge to users of shallow, privately tubed wells. It is difficult for these people to get enough water to satisfy their regular requirements. Additional practical consequences of this study include addressing a shortage of water, enhancing water usage and preservation oversight, assisting in the development of a strategic plan to address the enduring issue of water resource preservation, and giving priority to strategies for guaranteeing sustainable utilization of GW in regions with a significant amount of farming activity and comparable geographical and climatic features. The future goal for the GWP study is to look into how changes in climate, land use planning, and farming operations impact recharging zones. When developing recharging zone maps, use AI—machine learning and deep learning technologies—to improve modelling, estimation, and decision assistance. Prospective GWP studies must take into account the specific chemical makeup of various kinds of rocks, the trend of groundwater flow, the complex setting, and, certainly, the high installation expenses. The uncovered GWP zone maps of the data-scarce and disadvantaged area are going to offer the best solution for the public and private sectors to properly oversee and strategically organize the resource. Considering their superior and speedy effectiveness, the methodologies used show the efficacy of MLAs, remote sensing, and GIS in spatial multi-decision-making processes, particularly in addressing groundwater issues.

Abbreviation

AdaBoost	Adaptive Boosting
AHP	Analytical Hierarchy Process
AUC	Area Under Curve
AUROC	Area Under the Receiver Operating Characteristic
BH	Borehole
CI	Consistency Index
CR	Consistency Ratio
CRU	Climatic Research Unit
DD	Drainage Density
DEM	Digital Elevation Model
FN	Fishnet
FPR	False Positive Rate
GIS	Geographic Information System
GW	Groundwater
GWP	Groundwater Potential
GWPZ	Groundwater Potential Zones
GY	Geology
LD	Lineament Density
LL	Land use/Land cover
MC	Multicollinearity
MCDA	Multi-Criteria Decision Analysis
ML	Machine Learning
MLAs	ML Algorithms
MPC	mean percentage change
NDVI	Normalized Difference Vegetation Index
OOB	Out-of-Bag
PSW	Proximity to Surface Water Bodies
RBF	Radial Basis Function
RD	Rainfall Distribution
RF	Random Forest
RI	Random Index
ROC	Receiver Operating Characteristics
RS	Remote sensing

1072	SA	Sensitivity Analysis
1073	SDGs	Sustainable Development Goals
1074	SI	Sensitivity Index
1075	SP	Slope
1076	SRTM	Shuttle Radar Topography Mission
1077	SVM	Support Vector Machines
1078	T	Tolerance
1079	TPR	True True Positive Rate
1080	<td>Topographic Wetness Index</td>	Topographic Wetness Index
1081	VIF	Variance Inflation Factor
1082	XGB	eXtreme gradient boost

1083
1084

1085 References

- 1086 Abrams, W., Ghoneim, E., Shew, R., LaMaskin, T., Al-Bloushi, K., Hussein, S., AbuBakr, M., Al-Mulla, E., Al-Awar, M., El-
1087 Baz, F., 2018. Delineation of groundwater potential (GWP) in the northern United Arab Emirates and Oman using geospatial
1088 technologies in conjunction with Simple Additive Weight (SAW), Analytical Hierarchy Process (AHP), and Probabilistic
1089 Frequency Ratio (PFR) techniques. *J. Arid. Environ.* 157, 77–96. <https://doi.org/10.1016/j.jaridenv.2018.05.005>.
- 1090 Abrar, H., Kura, A.L., Dube, E.E. Beyene, D.L., 2021. AHP based analysis of groundwater potential in the western escarpment
1091 of the Ethiopian rift valley, *Geol. Ecol. Landsc.* 7 (3), 175–188. <https://doi.org/10.1080/24749508.2021.1952761>.
- 1092 Adewumi, J.R., Ajibade, T.F., Ajibade, F.O., 2020. Appraisal of on-site sanitation facilities and solid waste management in
1093 public places within Akure municipality, Nigeria. *J Civil Eng. Sci Technol.* 11 (1), 1–20. <https://doi.org/10.33736/jcest.1872.2020>.
- 1094 Agarwal, E., Agarwal, R., Garg, R.D., Garg, P.K., 2013. Delineation of groundwater potential zone: An AHP/ANP approach.
1095 *J Earth Syst Sci* 122, 887–898. <https://doi.org/10.1007/s12040-013-0309-y>.
- 1096 Ahmed, R., Sajjad, H., 2018. Analyzing factors of groundwater potential and its relation with population in the Lower Barpani
1097 Watershed, Assam, India. *Nat. Resour. Res.* 27, 503–515. <https://doi.org/10.1007/s11053-017-9367-y>.
- 1098 Ajay Kumar, V., Mondal, N.C., Ahmed, S., 2020. Identification of groundwater potential zones using RS, GIS and AHP
1099 techniques: a case study in a part of Deccan Volcanic Province (DVP), Maharashtra, India. *J Indian Soc Remote Sens* 48, 497–
1100 511. <https://doi.org/10.1007/s12524-019-01086-3>.
- 1101 Akinci, H., Ozalp, A.Y., Bülent, T., 2013. Agricultural Land Use Suitability using GIS and AHP Technique. *Comput. Electron.*
1102 *Agric.* 97, 71–82. <https://doi.org/10.1016/j.compag.2013.07.006>.
- 1103 Al-Djazouli, M.O., Elmorabiti, K., Rahimi, A., Amellah, O., Fadil, O.A.M., 2020. Delineating of groundwater potential zones
1104 based on remote sensing, GIS and analytical hierarchical process: a case of Waddai, eastern Chad. *GeoJournal.*
1105 <https://doi.org/10.1007/s10708-020-10160-0>.
- 1106 Ali, R., Sajjad, H., Saha, T.K., Roshani, Masroor, M., Rahaman, M.H., 2023. Effectiveness of machine learning ensemble
1107 models in assessing groundwater potential in Lidder watershed, India. *Acta Geophys.* 72, 2843–2856.
1108 <https://doi.org/10.1007/s11600-023-01237-8>.
- 1109 Alonso, J.A., Lamata, M.T., 2006. Consistency in the analytic hierarchy process: a new Approach. *Int. J. Uncertain. Fuzziness
Knowledge-Based Syst.* 14 (4), 445–459. <https://doi.org/10.1142/S0218488506004114>.
- 1110 Al-Shabeb, AA-R., Al-Adamat, R., Al-Fugara, A., Al-Amoush, H., AlAyyash, S., 2018. Delineating groundwater potential
1111 zones within the Azraq Basin of Central Jordan using multi-criteria GIS analysis. *Groundw Sustain Dev* 7, 82–90.
1112 <https://doi.org/10.1016/j.gsd.2018.03.011>.
- 1113 Arabameri, A., Pal, S.C., Rezaie, F., Nalivan, O.M., Chowdhuri, I., Saha, A., Lee, S., Moayedi, H., 2021. Modeling
1114 groundwater potential using novel GIS-based machine-learning ensemble techniques. *J Hydrol Reg Stud* 36, 100848.
1115 <https://doi.org/10.1016/j.ejrh.2021.100848>.
- 1116 Arefin, R., 2020. Groundwater potential zone identification using an analytic hierarchy process in Dhaka City, Bangladesh.
1117 *Environ. Earth Sci.* 79 (11), 268. <https://doi.org/10.1007/s12665-020-09024-0>.
- 1118 Arshad, A., Zhang, Z., Zhang, W., Dilawar, A., 2020. Mapping favorable groundwater potential recharge zones using a GIS-
1119 based analytical hierarchical process and probability frequency ratio model: A case study from an agro-urban region of
1120 Pakistan. *Geosci. Front.* 11, 1805–1819. <https://doi.org/10.1016/j.gsf.2019.12.013>.

- 1134 Avand, M., Janizadeh, S., Tien Bui, D., Pham, V.H., Ngo, P.T.T., Nhu, V.H., 2020. A tree-based intelligence ensemble approach
1135 for spatial prediction of potential groundwater. Int. J. Digit. Earth 13 (12), 1408–1429.
1136 <https://doi.org/10.1080/17538947.2020.1718785>.
- 1137 Baghel, S., Tripathi, M.P., Khalkho, D., Al-Ansari, N., Kumar, A., Elbeltagi, A., 2023. Delineation of suitable sites for
1138 groundwater recharge based on groundwater potential with RS, GIS, and AHP approach for Mand catchment of Mahanadi
1139 Basin. Sci. Rep. 13 (1), 9860. <https://doi.org/10.1038/s41598-023-36897-5>.
- 1140
- 1141 Breiman, L., 2001. Random Forests. Mach. Learn. 45, 5–32. <https://doi.org/10.1023/A:1010933404324>.
- 1142 Brunelli, M., 2015. Introduction to the Analytic Hierarchy Process. SpringerBriefs in Operations Research. Springer Cham.
1143 <https://doi.org/10.1007/978-3-319-12502-2>.
- 1144 Castillo, J.L., Martínez Cruz, D.A., Ramos Leal, J.A., Tuxpan Vargas, J., Rodriguez Tapia, S.A., Marín Celestino, A.E., 2022.
1145 Delineation of groundwater potential zones (GWPZs) in a semi-arid basin through remote sensing, GIS, and AHP approaches,
1146 Water 14 2138. <https://doi.org/10.3390/w14132138>
- 1147
- 1148 Chatterjee, D., Singh, P.K., Singh, D., Das, D.B., 2024. Implementation of Satellite-based Water Accounting Plus (WA+)
1149 Framework for Estimating Groundwater Balance and Utilization in a Semi-Arid River Basin of India. 28, 101391.
1150 <https://doi.org/10.1016/j.gsd.2024.101391>
- 1151
- 1152 Chen, W., Panahi, M., Khosravi, K., Pourghasemi, H.R., Rezaie, F., Parvinnezhad, D., 2019. Spatial prediction of groundwater
1153 potentiality using ANFIS ensembled with teaching-learning-based and biogeography-based optimization. J Hydrol 572, 435–
1154 448. <https://doi.org/10.1016/j.jhydrol.2019.03.013>.
- 1155 Chen, W., Li, H., Hou, E., Wang, S., Wang, G., Panahi, M., Li, T., Peng, T., Guo, C., Niu, C., 2018. GIS-based groundwater
1156 potential analysis using novel ensemble weights-of-evidence with logistic regression and functional tree models. Sci. Total
1157 Environ. 634, 853–867. <https://doi.org/10.1016/j.scitotenv.2018.04.055>.
- 1158
- 1159 Danumah, J.H., Odai, S.N., Saley, B.M., Szarzynski, J., Thiel, M., Kwaku, A., Kouame, F.K., Akpa, L.Y., 2016. Flood risk
1160 assessment and mapping in Abidjan district using multi-criteria analysis (AHP) model and geoinformation techniques, (Côte
1161 d'Ivoire). Geoenviron. Disasters 3, 10. <https://doi.org/10.1186/s40677-016-0044-y>.
- 1162
- 1163 Dar, T., Rai, N., Bhat, A., 2021. Delineation of potential groundwater recharge zones using analytical hierarchy process (AHP).
1164 Geol Ecol Landsc 5(4), 292–307. <https://doi.org/10.1080/24749508.2020.1726562>.
- 1165
- 1166 Das, S., 2019. Comparison among Influencing Factor, Frequency Ratio, and Analytical Hierarchy Process Techniques for
1167 Groundwater Potential Zonation in Vaitarna Basin, Maharashtra, India. Groundwater for Sustainable Development. 8, 617–
1168 629. <https://doi.org/10.1016/j.gsd.2019.03.003>.
- 1169 Dey, B., Abir, K.A., Ahmed, R., Salam, M.A., Redowan, M., Miah, M.D., Iqbal, M.A., 2023. Monitoring groundwater potential
1170 dynamics of north-eastern Bengal Basin in Bangladesh using AHP-Machine learning approaches. Ecological Indicators 154,
1171 110886. <https://doi.org/10.1016/j.ecolind.2023.110886>.
- 1172 Echogdali, F.Z., Boutaleb, S., Bendarma, A., Saidi, M.E., Aadraoui, M., Abiouei, M., Ouchchen, M., Abdelrahman, K., Fnais,
1173 M.S., Sajinkumar, K.S., 2022. Application of analytical hierarchy process and geophysical method for groundwater potential
1174 mapping in the Tata basin, Morocco. Water 14(15), 2393. <https://doi.org/10.3390/w14152393>.
- 1175
- 1176 Fajemilo, P.T., Ozegin, K.O., 2024. Evaluation of the groundwater potential of Ogbomoso, Southwestern Nigeria, using an
1177 adaptive neuro-fuzzy inference system optimized by three metaheuristic algorithms. Iran J Geophys. 8 (6), 47–78
1178 <https://doi.org/10.30499/ijg.2024.431927.1559>.
- 1179
- 1180 Freund, Y., Schapire, R.E., 1995. A decision-theoretic generalization of on-line learning and an application to boosting. In:
1181 Vítányi, P. (eds) Computational Learning Theory. EuroCOLT 1995. Lecture Notes in Computer Science, 904. Springer, Berlin,
1182 Heidelberg. <https://doi.org/10.1007/BFb002166>.
- 1183 Freund, Y., Schapire, R.E., 1997. A decision-theoretic generalization of on-line learning and an application to boosting. Journal
1184 of Computer and System Sciences 55, 119–139. <https://doi.org/10.1145/2818346.2823306>.
- 1185 Gayen, A., Pourghasemi, H.R., Saha, S., Keesstra, S., Bai, S., 2019. Gully Erosion Susceptibility Assessment and Management
1186 of Hazard-prone Areas in India Using Different Machine Learning Algorithms. Science of the Total Environment. 668, 124–
1187 138. <https://doi.org/10.1016/j.scitotenv.2019.02.436>.
- 1188
- 1189 Golkarian, A., Naghibi, S.A., Kalantar, B., Pradhan, B., 2018. Groundwater potential mapping using C5.0, random forest, and
1190 multivariate adaptive regression spline models in GIS. Environ. Monit. Assess. 190 (3), 149. <https://doi.org/10.1007/s10661-018-6507-8>.
- 1191

- 1192 Goward, S.N., Markham, B., Dye, D.G., Dulaney, W., Yang, J., 1991. Normalized difference vegetation index measurements
1193 from the advanced very high-resolution radiometer. *Remote Sensing of Environment* 35 (2-3), 257-277.
1194 [https://doi.org/10.1016/0034-4257\(91\)90017-Z](https://doi.org/10.1016/0034-4257(91)90017-Z).
- 1195 Guru, B., Seshan, K., Bera, S., 2017. Frequency ratio model for groundwater potential mapping and its sustainable management
1196 in cold desert, India. *J. King Saud Univ.-Sci.* 29 (3), 333-347. <https://doi.org/10.1016/j.jksus.2016.08.003>.
- 1197
- 1198 Hasanuzzaman, M., Mandal, M.H., Hasnine, M., Shit, P.K., 2022. Groundwater potential mapping sing multi-criteria decision,
1199 bivariate statistic and machine learning algorithms: evidence from Chota Nagpr Platea, India. *Appl Water Sci.* 12(4), 1-16.
1200 <https://doi.org/10.1007/s13201-022-01584-9>.
- 1201 Hong, H., Pradhan, B., Bui, D.T., Xu, C., Youssef, A.M., Chen, W., 2017. Comparison of Four Kernel Functions Used in
1202 Support Vector Machines for Landslide Susceptibility Mapping: A Case Study at Sichuan Area (China). *Geomatics, Natural
1203 Hazards and Risk.* 8(2), 544-569. <https://doi.org/10.1080/19475705.2016.1250112>.
- 1204
- 1205 Horn, R.A., Johnson, C.R., 1985. Matrix Analysis. Cambridge University Press.
1206 https://assets.cambridge.org/97805218/39402/frontmatter/9780521839402_frontmatter.pdf.
- 1207 Hussain, S., Mubeen, M., Ahmad, A., Majeed, H., Qaisrani, S.A., Hammad, H.M., Amjad, M., Ahmed, I., Fahhad, S., Ahmed,
1208 N., Nasim, W., 2022. Assessment of land use/land cover changes and its effect on land surface temperature using remote
1209 sensing techniques in Southern Punjab, Pakistan. *Environ. Sci. Pollution Res.*, 30, 99202-99218.
1210 <https://doi.org/10.1007/s11356-022-21650-8>.
- 1211
- 1212 Hutchinson, M.L., Antono, E., Gibbons, B.M., Paradiso, S., Ling, J., Meredig, B., 2017. Overcoming data scarcity with transfer
1213 learning. 31st Conference on Neural Information Processing Systems (NIPS 2017), Long Beach, CA, USA.
1214 <https://arxiv.org/abs/1711.05099v1>.
- 1215 Ikrri, M., Boutaleb, I., Abiou, M., Zahra, F.E., Abdelrahman, K., Mouna, I., Tamer, A., Hasna, E.A., Sara, E., Farid, F. 2023.
1216 Delineation of groundwater potential area using an AHP, remote sensing, and GIS Techniques in the Ifni Basin, Western Anti-
1217 Atlas, and Morocco. *Water* 15(7), 1436. <https://doi.org/10.3390/w15071436>.
- 1218
- 1219 Ilugbo, S.O., Aigbedion, I., Ozegin, K.O., Bawallah, M.A., 2023a. Assessment of groundwater occurrence in a typical schist
1220 belt region in Osun state, southwestern Nigeria using VES, aeromagnetic dataset, remotely sensed data and MCDA approaches.
1221 *Sustain. Water Resourc. Manag.* 9, 29. <https://doi.org/10.1007/s40899-022-00810-1>.
- 1222 Ilugbo, S.O., Aigbedion, I., Ozegin, K.O., 2023b. Structural mapping for groundwater occurrence using remote sensing and
1223 geophysical data in Ilesha Schist Belt, Southwestern Nigeria. *Geology, Ecology, and Landscapes.*
1224 <https://doi.org/10.1080/24749508.2023.2182063>.
- 1225
- 1226 Ilugbo, S.O., Ozegin, K.O., 2018. Significances of Deep-Seated Lineament in Groundwater Studies around Ilesha,
1227 Southwestern Nigeria. *Asian Journal of geological Research* 1 (1), 1-16. <https://doi.org/10.9734/AJGER/2018/42078>.
- 1228
- 1229 Jennifer, J.J., 2022. Feature elimination and comparison of machine learning algorithms in landslide susceptibility mapping.
1230 *Environ Earth Sci.* 81, 489. <https://doi.org/10.1007/s12665-022-10620-5>.
- 1231 Kalura, P., Pandey, A., Chowdary, V.M., Raju, P.V., 2022. Land Use Land Cover Change Detection of the Tons River Basin
1232 Using Remote Sensing and GIS. In: Pandey, A., Chowdary, V.M., Behera, M.D., Singh, V.P. (eds) Geospatial Technologies for
1233 Land and Water Resources Management. *Water Science and Technology Library*, 103, 53-65. Springer, Cham.
1234 https://doi.org/10.1007/978-3-030-90479-1_4.
- 1235
- 1236 Karimi-Rizvandi, S., Goodarzi, H.V., Afkouieh, J.H., Chung, I-M., Kisi, O., Kim, S., 2021. Groundwater-potential mapping
1237 using a self-learning bayesian network model: a comparison among metaheuristic algorithms. *Water* 13, 658.
1238 <https://doi.org/10.3390/w13050658>.
- 1239 Kavzoglu, T., Colkesen, I., Sahin, E.K., 2019. Machine Learning Techniques in Landslide Susceptibility Mapping: a Survey
1240 and a Case Study. Springer, Cham, 50, 283-301. https://doi.org/10.1007/978-3-319-77377-3_13.
- 1241
- 1242 Kaya, Y.; Sanli, F.B.; Abdikan, S., 2023. Determination of long-term volume change in lakes by integration of UAV and
1243 satellite data: The case of Lake Burdur in Türkiye. *Environ. Sci. Pollut. Res. Int.* 30, 117729-117747.
1244 <https://doi.org/10.1007/s11356-023-30369-z>.
- 1245 Khan, Q., Liaqat, M.U., Mohamed, M.M., 2021. A comparative assessment of modeling groundwater vulnerability using
1246 DRASTIC method from GIS and a novel classification method using machine learning classifiers. *Geocarto International.*
1247 37(20), 5832-5850. <https://doi.org/10.1080/10106049.2021.1923833>.
- 1248 Khan, Z.A., Jhamnani, B., 2023. Identification of groundwater potential zones of Idukki district using remote sensing and GIS-
1249 based machine-learning approach. *Water Supply* 23 (6), 2426. <https://doi.org/10.2166/ws.2023.134>.

- 1250 Kolawole, A.O., 2015. Nigeria's Water Resources and Spatial Variation in Water Quality. Department of Environmental
1251 Quality Sciences, The Hebrew University of Jerusalem. <https://doi.org/10.13140/RG.2.1.2843.9209>. Technical Report, March.
1252
- 1253 Kroll, C.N., Song, P., 2013. Impact of multicollinearity on small sample hydrologic regression models. *Water Resour. Res.* 49,
1254 3756–3769. <https://doi.org/10.1002/wrcr.20315>.
- 1255 Lee, S., Hong S-M., Jung, H.S., 2018. GIS-based groundwater potential mapping using artificial neural network and support
1256 vector machine models: the case of boryeong city in Korea. *Geocarto Int.* 33(8), 847–861.
1257 <https://doi.org/10.1080/10106049.2017.1303091>.
- 1258
- 1259 Lee, S., Song, K-Y., Kim, Y., Park, I., 2012. Regional groundwater productivity potential mapping using a geographic
1260 information system (GIS) based artificial neural network model. *Hydrogeol J* 20, 1511–1527. <https://doi.org/10.1007/s10040-012-0894-7>.
- 1261
- 1262 Lee, S., Hyun, Y., Lee, S., Lee, M.J., 2020. Groundwater potential mapping using remote sensing and GIS-based machine
1263 learning techniques. *Remote Sens.* 12(7), 1200. <https://doi.org/10.3390/rs12071200>.
- 1264
- 1265 Liaw, A., Wiener., M., 2024. Breiman and Cutler's Random Forests for Classification and Regression. Available online:
<https://cran.r-project.org/web/packages/randomForest/randomForest.pdf> (accessed on 15 April 2025).
- 1266
- 1267 Maity, D.K., Mandal, S., 2019. Identification of Groundwater potential zones of the Kumari River Basin, India: an RS & GIS
1268 based Semi-quantitative Approach. *Environ Dev Sustain* 21(2), 1013– 1034. <https://doi.org/10.1007/s10668-017-0072-0>.
- 1269
- 1270 Malczewski, J., 2010. Multiple Criteria Decision Analysis and Geographic Information Systems. In: Ehrgott, M., Figueira, J.,
1271 Greco, S. (eds) Trends in Multiple Criteria Decision Analysis. International Series in Operations Research & Management
1272 Science 142, 369–395. Springer, Boston, MA. https://doi.org/10.1007/978-1-4419-5904-1_13.
- 1273
- 1274 Mandal, P., Saha, J., Bhattacharya, S., Paul, S., 2021. Delineation of groundwater potential zones using the integration of
1275 geospatial and MIF techniques: A case study on Rarh region of West Bengal, India. *Environ. Chall.* 5, 100396.
1276 <https://doi.org/10.1016/j.envc.2021.100396>.
- 1277
- 1278 Mansour, S., Al-Awhadi, T., Al-Hatrushi, S., 2019. Geospatial based Multi-criteria Analysis for Ecotourism Land Suitability
1279 using GIS and AHP: A Case Study in Masirah Island, Oman. *J. Ecotourism.* 19(2), 148-167.
1280 <https://doi.org/10.1080/14724049.2019.1663202>.
- 1281
- 1282 Marjanović, M., Kovačević, M., Bajat, B., Vozenilek, V., 2011. Landslide Susceptibility Assessment Using SVM Machine
1283 Learning Algorithm. *Engineering Geology.* 123(3), 225–234. <https://doi.org/10.1016/j.enggeo.2011.09.006>.
- 1284
- 1285 Maskooni, E.K., Naghibi, S.A., Hashemi, H., Berndtsson, R., 2020. Application of advanced machine learning algorithms to
assess groundwater potential using remote sensing-derived data. *Remote Sens* 12, 2742. <https://doi.org/10.3390/rs12172742>.
- 1286
- 1287 Masroor, M., Sajjad, H., Kumar, P., Saha, T.K., Rahaman, M.H., Choudhari, P., Kulimushi, L.C., Pal, S., Saito, O., 2023. Novel
1288 ensemble machine learning modeling approach for groundwater potential mapping in Parbhani District of Maharashtra, India.
Water 15 (3), 419. <https://doi.org/10.3390/w15030419>.
- 1289
- 1290 Mathewos, Y., Abate, B., Dadi, M., Mathewos, M., 2024. Evaluation of the groundwater prospective zone by coupling hydro-
1291 meteorological and geospatial evidence in Wabe River Catchment Omo Gibe River Basin, Ethiopia. *Water Cycle* 5, 37–58.
1292 <https://doi.org/10.1016/j.watcyc.2024.01.002>.
- 1293
- 1294 McKay, G., Harris, J.R., 2016. Comparison of the data-driven random forests model and a knowledge-driven method for
1295 mineral prospectively mapping: a case study for gold deposits around the Huritz Group and Nueltin Suite, Nunavut, Canada.
1296 *Nat Resour Res.* 25, 125–143. <https://doi.org/10.1007/s11053-015-9274-z>.
- 1297
- 1298 Moghaddam, D.D., Rahmati, O., Haghizadeh, A., Kalantari, Z.A., 2020. A modeling comparison of groundwater potential
1299 mapping in a mountain bedrock aquifer: QUEST, GARP, and RF models. *Water* 12(3), 679. <https://doi.org/10.3390/w12030679>.
- 1300
- 1301 Mohammadi-Behzad, H.R., Charchi, A., Kalantari, N., Nejad, A.M., Vardanjani, H.K., 2019. Delineation of groundwater
1302 potential zones using remote sensing (RS), geographical information system (GIS) and analytic hierarchy process (AHP)
1303 techniques: A case study in the Leylia–Keynow watershed, southwest of Iran. *Carbonates Evaporites.* 34, 1307–1319.
1304 <https://doi.org/10.1007/s13146-018-0420-7>.
- 1305
- 1306 Morales, F., Jr., de Vries, W.T., 2021. Establishment of Land Use Suitability Mapping Criteria Using Analytic Hierarchy
1307 Process (AHP) with Practitioners and Beneficiaries. *Land* 10, 235. <https://doi.org/10.3390/land10030235>.

- 1308 Morbidelli, R., Saltalippi, C., Flammini, A., Govindaraju R.S., 2018. Role of slope on infiltration: a review. J.
1309 Hydrol. 557, 878-886. <https://doi.org/10.1016/j.jhydrol.2018.01.019>.
- 1310 Mukherjee, I., Singh, U., 2020. Delineation of groundwater potential zones in a drought prone semi-arid region of east India
1311 using GIS and analytical hierarchical process techniques. Catena 194, 104681. <https://doi.org/10.1016/j.catena.2020.104681>.
- 1312 Muthu, K., Sudalaimuthu, K., 2021. Integration of Remote sensing, GIS, and AHP in demarcating groundwater potential zones
1313 in Pattukkottai Taluk, Tamilnadu, India, Arabian J. Geosci. 14, 1748. <https://doi.org/10.1007/s12517-021-08110-2>.
- 1314 Naghibi, S.A., Pourghasemi, H.R., 2015. A comparative assessment between three machine learning models and their
1315 performance comparison by bivariate and multivariate statistical methods in groundwater potential mapping. Water Resour
1316 Manag. 29, 5217–5236. <https://doi.org/10.1007/s11269-015-1114-8>.
- 1317 Naghibi, S.A., Pourghasemi, H.R., Dixon, B., 2016. GIS-based groundwater potential mapping using boosted regression tree,
1318 classification and regression tree, and random forest machine learning models in Iran. Environ. Monit. Assess. 188, 44.
<https://doi.org/10.1007/s10661-015-5049-6>.
- 1319 Naghibi, S.A., Kourosh Ahmadi, K., Daneshi, A., 2017. Application of Support Vector Machine, Random Forest, and Genetic
1320 Algorithm Optimized Random Forest Models. Water Resour Manage 31, 2761–2775. [https://doi.org/10.1007/s11269-017-1660-3](https://doi.org/10.1007/s11269-017-
1321 1660-3).
- 1322 Naghibi, S.A., Pourghasemi, H.R., Abbaspour, K., 2018. A Comparison between Ten Avance an Soft Computing Models for
1323 Groundwater Qanat Potential Assessment in Iran Using R an GIS. Theoretical and Applied Climatology. 131, 967–984.
<https://doi.org/10.1007/s00704-016-2022-4>.
- 1324 Naghibi, S.A., Hashemi, H., Berndtsson, R., Lee, S., 2020. Application of extreme gradient boosting and parallel random forest
1325 algorithms for assessing groundwater spring potential using DEM-derived factors, J. Hydrol. 589, 125197.
<https://doi.org/10.1016/j.jhydrol.2020.125197>.
- 1326 Niazkar, M., Menapace, A., Brentan, B., Piraei, R., Jimenez, D., Dhawan, P., Righetti, M., 2024. Applications of XGBoost in
1327 water resources engineering: a systematic literature review (Dec 2018–May 2023). Environ. Model. Softw. 174, 105971.
<https://doi.org/10.1016/j.envsoft.2024.105971>.
- 1328 Obaje, N.G. 2009. The Basement Complex. In: Geology and Mineral Resources of Nigeria. Lecture Notes in Earth Sciences.
1329 120. Springer, Berlin, Heidelberg. https://doi.org/10.1007/978-3-540-92685-6_2.
- 1330 Odeyemi, I.B., 1981. A review of orogenic events in the Precambrian Basement of Nigeria, West Africa. Geol Rundsch.
1331 70(3):897–909. <https://doi.org/10.1007/BF01820170>.
- 1332 Oh, H. J., Kim, Y.S., Choi, J.K., Park, E., Lee, S., 2011. GIS Mapping of Regional Probabilistic Groundwater Potential in the
1333 Area of Pohang City, Korea. Journal of Hydrology 399 (3–4), 158–172. <https://doi.org/10.1016/j.jhydrol.2010.12.027>.
- 1334 Olden, J.D., Lawler, J.J., Poff, N.L., 2008. Machine learning methods without tears: a primer for ecologists. Quarterly Review
1335 of Biology 83, 171–193. <https://doi.org/10.1086/587826>.
- 1336 Opoku, P.A., Shu, L., Amoako-Nimako, G.K., 2024. Assessment of Groundwater Potential Zones by Integrating
1337 Hydrogeological Data, Geographic Information Systems, Remote Sensing, and Analytical Hierarchical Process Techniques in
1338 the Jinan Karst Spring Basin of China. Water 16, 566. <https://doi.org/10.3390/w16040566>.
- 1339 Ozdemir, A., 2011. GIS-based groundwater spring potential mapping in the Sultan Mountains (Konya, Turkey) using frequency
1340 ratio, weights of evidence and logistic regression methods and their comparison. J. Hydrol. 411 (3-4), 290–308.
<https://doi.org/10.1016/j.jhydrol.2011.10.010>.
- 1341 Ozegin, K.O., Ilugbo, S.O., Ogunseye, T.T., 2023. Groundwater exploration in a landscape with heterogeneous geology: an
1342 application of geospatial and analytical hierarchical process (AHP) techniques in the Edo north region, in Nigeria.
Groundwater for Sustainable Development 20, 100871. <https://doi.org/10.1016/j.gsd.2022.100871>.
- 1343 Ozegin, K.O., Ilugbo, S.O., 2024. A triangulation approach for groundwater potential evaluation using geospatial technology
1344 and multi-criteria decision analysis (MCDA) in Edo State, Nigeria. J. Afr. Earth Sci. 209, 105101.
<https://doi.org/10.1016/j.jafrearsci.2023.105101>.
- 1345 Ozegin, K.O., Ilugbo, S.O., Akande, O.N., 2024a. Leveraging geospatial technology and AHP for groundwater potential
1346 zonation in parts of south and north-Central Nigeria. Sustainable Water Resources Management. 10, 146.
<https://doi.org/10.1007/s40899-024-01124-0>.
- 1347

- 1365 Ozegin, K.O., Ilugbo, S.O., Alile, O.M., Iluore, K., 2024b. Integrating in-situ data and spatial decision support systems (SDSS)
1366 to identify groundwater potential sites in the Esan plateau, Nigeria. *Groundwater for Sustainable Development* 26, 101276.
1367 <https://doi.org/10.1016/j.gsd.2024.101276>.
- 1368 Ozegin, K.O., Ilugbo, S.O., Adebo, B., 2024c. Spatial evaluation of groundwater vulnerability using the DRASTIC-L model
1369 with the analytic hierarchy process (AHP) and GIS approaches in Edo State, Nigeria. *Phys. Chem. Earth* 134, 103562.
1370 <https://doi.org/10.1016/j.pce.2024.103562>.
- 1371 Ozegin, K.O., Ilugbo, S.O., 2025. Evaluation of potentially susceptible flooding areas leveraging geospatial technology with
1372 multicriteria decision analysis in Edo State, Nigeria. *Natural Hazards Research.* 5 (1), 109-133.
1373 <https://doi.org/10.1016/j.nhres.2024.07.002>
- 1374 Pande, C.B., Moharir, K.N., Singh, S.K., Varade, A.M., 2020. An integrated approach to delineate the groundwater potential
1375 zones in Devdari watershed area of Akola district, Maharashtra, Central India. *Environ. Dev. Sustain.* 22 (5), 4867–4887.
1376 <https://doi.org/10.1007/s10668-019-00409-1>.
- 1377 Patidar, R., Pingale, S.M. Khare, D., 2021. An integration of geospatial and machine learning techniques for mapping
1378 groundwater potential: a case study of the Shipra River basin, India. *Arab J Geosci* 14, 1645. <https://doi.org/10.1007/s12517-021-07871-0>.
- 1379 Patra, S., Mishra, P., Mahapatra, S.C., 2018. Delineation of groundwater potential zone for sustainable development: A case
1380 study from Ganga Alluvial Plain covering Hooghly district of India using remote sensing, geographic information system and
1381 analytic hierarchy process. *Journal of Cleaner Production*, 172, 20 2485-2502. <https://doi.org/10.1016/j.jclepro.2017.11.161>.
- 1382 Pham, B.T., Jaafari, A., Phong, T.V., Mafi-Gholami, D., Amiri, M., Van Tao, N., Duong, V.-H., Prakash, I., 2021. Naïve Bayes
1383 ensemble models for groundwater potential mapping. *Ecol. Inform.* 64, 101389. <https://doi.org/10.1016/j.ecoinf.2021.101389>.
- 1384 Pourtaghi, Z.S., Pourghasemi, H.R., 2014. GIS-based groundwater spring potential assessment and mapping in the Birjand
1385 Township, southern Khorasan Province, Iran. *Hydrogeol J.* 22(3), 643–662. <https://doi.org/10.1007/s10040-013-1089-6>.
- 1386 Prasad, P., Loveson, V.J., Kotha, M., Yadav, R., 2020. Application of Machine Learning Techniques in Groundwater Potential
1387 Mapping along the West Coast of India. *Gisci. Remote Sens.* 57 (6), 735–752.
1388 <https://doi.org/10.1080/15481603.2020.1794104>.
- 1389 Rahmati, O., Pourghasemi, H.R., Melesse, A.M., 2016. Application of GIS-based data driven random forest and maximum
1390 entropy models for groundwater potential mapping: a case study at Mehran region, Iran. *Catena* 137, 360–372.
1391 <https://doi.org/10.1016/j.catena.2015.10.010>.
- 1392 Rahmati, O., Melesse, A.M., 2016. Application of Dempster-Shafer theory, spatial analysis and remote sensing for groundwater
1393 potentiality and nitrate pollution analysis in the semi-arid region of Khuzestan, Iran. *Sci. Total Environ.* 568, 1110–1123.
1394 <https://doi.org/10.1016/j.scitotenv.2016.06.176>.
- 1395 Rahmati, O., Pourghasemi, H.R., Melesse, A.M., 2016. Application of GIS-based data driven random forest and maximum
1396 entropy models for groundwater potential mapping: A case study at Mehran Region, Iran. *Catena*, 137, 360–372.
1397 <https://doi.org/10.1016/j.catena.2015.10.010>.
- 1398 Rajaveni, S.P., Brindha, K., Elango, L., 2017. Geological and Geomorphological Controls on Groundwater Occurrence in a
1399 Hard Rock Region. *Applied Water Science.* 7(3), 1377–1389. <https://doi.org/10.1007/s13201-015-0327-6>.
- 1400 Rajendran, G., Mohammed, M., Shivakumar, S., Merera, W., Taddese, K., 2020. Geospatial techniques amalgamated with
1401 two-dimensional electrical resistivity imaging for delineation of groundwater potential zones in West Guji Zone, Ethiopia,
1402 *Groundwater Sustain. Dev.* 11 (2020) 100407, <https://doi.org/10.1016/j.gsd.2020.100407>.
- 1403 Rana, M.M.S.P., Rahman, M.T., Hassan, M.F., 2025. Mapping groundwater potential zone by robust machine learning
1404 algorithms & remote sensing techniques in agriculture dominated area, Bangladesh. *Cleaner Water* 3, 100064.
1405 <https://doi.org/10.1016/j.clwat.2025.100064>.
- 1406 Rao, N.S., Gugulothu, S., Das, R., 2022. Deciphering artificial groundwater recharge suitability zones in the agricultural area
1407 of a river basin in Andhra Pradesh, India using geospatial techniques and analytical hierarchical process method. *Catena* 212,
1408 106085. <https://doi.org/10.1016/j.catena.2022.106085>
- 1409 Razavi-Termeh, S.V., Sadeghi-Niaraki, A., Choi, S.M., 2019. Groundwater potential mapping using an integrated ensemble of
1410 three bivariate statistical models with random forest and logistic model tree models. *Water* 11(8),
1411 1596. <https://doi.org/10.3390/w11081596>.
- 1412
- 1413
- 1414
- 1415
- 1416
- 1417
- 1418
- 1419
- 1420
- 1421
- 1422
- 1423
- 1424

- 1425 Reza, A., Seiyed, S., Hosseini, M., 2023. Assessment and delineation of potential groundwater recharge zones in areas prone
1426 to saltwater intrusion hazard: A case from Central Iran. Environ. Monit. Assess. 195, 203. <https://doi.org/10.1007/s10661-022-10778-2>.
- 1427
- 1428 Roy, A., Keesari, T., Sinha, U.K., Sabarathinam, C., 2019. Delineating groundwater prospect zones in a region with extreme
1429 climatic conditions using GIS and remote sensing techniques: A case study from central India. Journal of Earth System Science,
1430 128, 1–19. <https://doi.org/10.1007/s12040-019-1205-7>.
- 1431
- 1432 Saaty, T.L., 1990. How to make a decision: the Analytic hierarchy process. Eur. J. Oper. Res. 48, 9–26.
1433 [https://doi.org/10.1016/0377-2217\(90\)90057-I](https://doi.org/10.1016/0377-2217(90)90057-I).
- 1434
- 1435 Sachdeva, S., Kumar, B., 2021. Comparison of gradient boosted decision trees and random forest for groundwater potential
1436 mapping in Dholpur (Rajasthan), India. Stochastic Environmental Research and Risk Assessment 35 (2), 287–306.
1437 <https://doi.org/10.1007/S00477-020-01891-0/TABLES/6>.
- 1438
- 1439 Saha, S., 2017. Groundwater potential mapping using analytical hierarchical process: a study on Md. Bazar Block of Birbhum
1440 District, West Bengal. Spatial Information Research 25 (4), 615–626. <https://doi.org/10.1007/s41324-017-0127-1>.
- 1441
- 1442 Saha, R., Baranval, N.K., Das, I., Kumaranchat, V.K., Reddy, K.S., 2022. Application of machine learning and geospatial
1443 techniques for groundwater potential mapping. J Ind Soc Remote Sensing 50(10), 1995–2010. <https://doi.org/10.1007/s12524-022-01582-z>.
- 1444
- 1445 Saha, B., Acharya, T., Sur, T., 2024. Delineation of groundwater potential zones in coastal alluvial region using remote sensing,
1446 geographic information system and analytical hierarchy process techniques. 26, 101238.
1447 <https://doi.org/10.1016/j.gsd.2024.101238>.
- 1448
- 1449 Sahoo, S., Russo, T.A., Elliott, J., Foster, I., 2017. Machine learning algorithms for modeling groundwater level changes in
1450 agricultural regions of the U.S. Water Resour. Res. 53 (5), 3878–3895. <https://doi.org/10.1002/2016WR019933>.
- 1451
- 1452 Sameen, M.I., Pradhan, B., Lee, S., 2019. Self-learning random forests model for mapping groundwater yield in data-scarce
1453 areas. Nat. Resour. Res. 28, 757–775. <https://doi.org/10.1007/s11053-018-9416-1>.
- 1454
- 1455 Samui, P., 2008. Slope Stability Analysis: A Support Vector Machine Approach. Environ. Geol. 56(2), 255–267.
1456 <https://doi.org/10.1007/s00254-007-1161-4>.
- 1457 Scanlon, B.R., Fakhreddine, S., Rateb, A., de Graaf, I., Famiglietti, J., Gleeson, T., Grafton, R.Q., Jobbagy, E.C., Kebede, S.
1458 Kolusu, S.R., 2023. Global water resources and the role of groundwater in a resilient water future, Nature Reviews Earth &
1459 Environment, 4 (2), 87–101. <https://doi.org/10.1038/s43017-022-00378-6>.
- 1460
- 1461 Senanayake, I.P., Dissanayake, D.M.D.O.K., Mayadunna, B.B., Weerasekera, W.L., 2016. An approach to delineate
1462 groundwater recharge potential sites in Ambalantota, Sri Lanka using GIS techniques. Geosci. Front. 7, 115–124.
1463 <https://doi.org/10.1016/j.gsf.2015.03.002>.
- 1464
- 1465 Senapati, U., Das, T.K., 2021. Assessment of basin-scale groundwater potentiality mapping in drought-prone upper
1466 Dwarakeshwar River basin, West Bengal, India, using GIS-based AHP techniques. Arabian J. Geosci. 14 (11), 1–22.
1467 <https://doi.org/10.1007/s12517-021-07316-8>.
- 1468
- 1469 Shahinuzzaman, M., Haque, M.N., Shahid, S., 2021. Delineation of groundwater potential zones using a parsimonious concept
1470 based on catastrophe theory and analytical hierarchy process. Hydrgeol. J. 29, 1091–1116. <https://doi.org/10.1007/s10040-021-02322-2>.
- 1471
- 1472 Shandu, I.D., Atif, I., 2023. An Integration of Geospatial Modelling and Machine Learning Techniques for Mapping
1473 Groundwater Potential Zones in Nelson Mandela Bay, South Africa. Water 15, 3447. <https://doi.org/10.3390/w15193447>.
- 1474
- 1475 Sharma, R., Pandey, R.K., Singh, A.K., 2024. A Multi-criterian Approach to Identify Groundwater Potential Zones in the
1476 Subarnarekha River Basin Using Integrated Analytical Hierarchy Process and Geospatial Technology, Journal of Geography,
1477 Environment and Earth Science International, 28 (10), 78–100. <https://doi.org/10.9734/jgeesi/2024/v28i10827>.
- 1478
- 1479 Sharma, Y., Ahmed, R., Saha, T.K., Bhuyan, N., Kumari, G., Roshani, Pal S., Sajja, H., 2024. Assessment of groundwater
1480 potential and determination of influencing factors using remote sensing and machine learning algorithms: a study of Nainital
1481 district of Uttarakhand state, India. Groundw. Sustain. Dev. 25, 101094 <https://doi.org/10.1016/j.gsd.2024.101094>.
- 1482
- 1483 Singh, L.K., Jha, M.K., Chowdary, V.M., 2016. Multi-criteria analysis and GIS modeling for identifying prospective water
1484 harvesting and artificial recharge sites for sustainable water supply. J. Clean. Prod. 142, 1436–1456.
1485 <https://doi.org/10.1016/j.jclepro.2016.11.163>.

- 1486 Singha, C., Swain, K.C., Pradhan, B., Rusia D.K., Moghimi, A., Ranjgar, B., 2024. Mapping groundwater potential zone in
1487 the subarnarekha basin, India, using a novel hybrid multi-criteria approach in Google earth Engine. *Heliyon* 10, e24308.
1488 <https://doi.org/10.1016/j.heliyon.2024.e24308>.
- 1489
1490 Sinha, D.D., Mohapatra, S.N., Pani, P., 2012. Mapping and assessment of groundwater potential in Bilrai watershed (Shivpuri
1491 District, M.P.) a geomatics approach. *J. Indian Soc. Remote Sens.* 40, 649–668. <https://doi.org/10.1007/s12524-011-0175-2>.
- 1492
1493 Solomon, S., Quiel, F., 2006. Groundwater study using remote sensing and geographic information systems (GIS) in the central
1494 highlands of Eritrea. *Hydrogeol. J.* 14 (6), 1029–1041. <https://doi.org/10.1007/s10040-006-0096-2>.
- 1495
1496 Sørensen, R., Zinko, U., Seibert, J., 2006. On the calculation of the topographic wetness index: evaluation of different methods
1497 based on field observations. *Hydrol. Earth Syst. Sci.* 10, 101–112. <https://doi.org/10.5194/hess-10-101-2006>.
- 1498
1499 Tehrany, M.S., Pradhan, B., Mansor, S., Ahmad, N., 2015. Flood Susceptibility Assessment Using GIS-based Support Vector
1500 Machine Moel with Different Kernel Types. *Catena*. 125, 91–101. <https://doi.org/10.1016/j.catena.2014.10.017>.
- 1501
1502 Tucker, C.J., 1979. Red and photographic infrared linear combinations for monitoring vegetation. *Remote Sens Environ* 8(2),
1503 127–150. [https://doi.org/10.1016/0034-4257\(79\)90013-0](https://doi.org/10.1016/0034-4257(79)90013-0).
- 1504
1505 Thanh, N.N., Chotpantarat, S., Trung, N.H., Ngu, N.H., Muoi, L.N., 2022. Mapping groundwater potential zones in
1506 Kanchanaburi Province, Thailand by integrating of analytic hierarchy process, frequency ratio, and random forest. *Ecol.*
1507 *Indicat.* 145, 109591. <https://doi.org/10.1016/j.ecolind.2022.109591>.
- 1508
1509 UN DESA, 2022. United Nations department of economic and social affairs, population division. In: World Population
1510 Prospects 2022: Summary of Results. UN DESA/POP/2022/TR/NO.3.
1511 <https://www.un.org/development/desa/pd/content/World-Population-Prospects-2022>. (accessed on 5 April 2025).
- 1512
1513 UN DESA. SDGs Report 2023. The Sustainable Development Goals Report 2023: Special Edition. 2023, p. 80. Available
1514 online: <https://unstats.un.org/sdgs/report/2023/> (accessed on 9 February 2024).
- 1515
1516 United Nations, 2015. The UN 2030 agenda for sustainable development. Sustainable Development Goals Series.
1517 https://doi.org/10.1007/978-3-031-07461-5_1.
- 1518
1519 United Nations, 2023. The sustainable development goals report 2023: special Edition. <https://unstats.un.org/sdgs/report/2023/>.
- 1520 UNWWDR (UN World Water Development Report), 2022. Groundwater: Making the Invisible Visible.
1521 <https://www.unesco.org/reports/wwdr/2022/en/download>. (Accessed 17 January 2024).
- 1522
1523 UNWWDR (The United Nations World Water Development Report) 2025. Mountains and glaciers: water towers. UNESCO,
1524 Paris. <https://doi.org/10.54679/LHPJ5153>.
- 1525
1526 Vafadar, S., Rahimzadegan, M., Asadi, R., 2023. Evaluating the performance of machine learning methods and geographic
1527 information system (GIS) in identifying groundwater potential zones in Tehran-Karaj plain, Iran. *J. Hydrol.* 624, 129952.
<https://doi.org/10.1016/j.jhydrol.2023.129952>.
- 1528
1529 van der Gun, J., 2012. Groundwater and Global Change: Trends, Opportunities and Challenges. United Nations Educational,
1530 Scientific, and Cultural Organization, Paris, France, 44. <https://unesdoc.unesco.org/ark:/48223/pf0000215496>.
- 1531
1532 Venkatesh, S., Parimalarenganayaki, S., 2023. Multi-collinearity-based parameter optimization and comparison among multi-
1533 criteria decision analysis to map groundwater potential zones. *J. Geol. Soc. India* 99 (8), 1158–1164.
<https://doi.org/10.1007/s12594-023-2441-7>.
- 1534
1535 Venkatramanan, S., Prasanna, M.V., Chung, S.Y., 2019. GIS and geostatistical techniques for groundwater science. In:
1536 introduction and history of GIS and Geostatistical Techniques for Groundwater Science. <https://doi.org/10.1016/C2017-0-02667-8>.
- 1537
1538 Wang, J., Chen, L., Yu, Z., 2018. Modeling rainfall infiltration on hillslopes using flux-concentration relation and
1539 time compression approximation. *J. Hydrol.* 557, 243–253. <https://doi.org/10.1016/j.jhydrol.2017.12.031>.
- 1540
1541 Wiesmeier, M., Barthold, F., Blank, B., Kögel-Knabner, I., 2011. Digital Mapping of Soil Organic Matter Stocks Using
1542 Random Forest Modeling in a Semi-Arid Steppe Ecosystem. *Plant Soil* 340, 7–24. <https://doi.org/10.1007/s11104-010-0425-z>.
- 1543
1544 Wind, Y., Saaty, T.L., 1980. Marketing applications of the analytic hierarchy process. *Manag Sci* 26(7), 641–658
1545 <https://doi.org/10.1287/mnsc.26.7.641>.
- 1546

- 1547 World Bank Group, 2017. Report: a wake-up call: Nigeria water supply, sanitation, and hygiene poverty diagnostic. In: WASH
1548 Poverty Diagnostic Series. 2017 International Bank for Reconstruction and Development/The World Bank.
1549 <http://documents.worldbank.org/curated/en/56638.15023.79018.228/pdf/118241-WP-PUBLICWASH-series.pdf>. (Accessed 7
1550 July 2022)
- 1551
1552 WWQA (World Water Quality Alliance). 2021. Assessing Groundwater Quality: A Global Perspective: Importance, Methods
1553 and Potential Data Sources. A Report by the Friends of Groundwater in the World Water Quality Alliance. Information
1554 document annex for display at the 5th session of the United Nations Environment Assembly, Nairobi. 2021. [1555
\[igrac.org/data/resources/assessing-groundwater-quality-a-global-perspective/\]\(https://un-\)](https://un-)
- 1556 Yao, X., Tham, L.G., Dai., F.C., 2008. Landslide Susceptibility Mapping Based on Support Vector Machine: A Case Study on
1557 Natural Slopes of Hong Kong, China. Geomorphology. 101(4), 572–582. <https://doi.org/10.1016/j.geomorph.2008.02.011>.
- 1558
1559 Zabihi, M., Pourghasemi, H.R., Pourtaghi, Z.S., Behzadfar, M., 2016. GIS-based multivariate adaptive regression spline and
1560 random forest models for groundwater potential mapping in Iran. Environ. Earth Sci. 75 (8), 1–19.
1561 <https://doi.org/10.1007/s12665-016-5424-9>.
- 1562
1563 Zewdie, M.M., Kasie, L.A., Bogale, S., 2024. Groundwater potential zones delineation using GIS and AHP techniques in upper
1564 parts of Chemoga watershed, Ethiopia. Appl. Water Sci. 14 (4), 85. <https://doi.org/10.1007/s13201-024-02119-0>.
- 1565
1566 Zhang, Q., Zhang, S., Zhang, Y., Li, M., Wei, Y., Chen, M., Zhang, Z., Dai, Z., 2021. GIS-based groundwater potential
1567 assessment in varied topographic areas of Mianyang city, Southwestern China, using AHP, Rem. Sens. 13, 4684.
1568 <https://doi.org/10.3390/rs13224684>.
- 1569 Zhao, R., Fan, C. Arabameri, A., Santosh, M., Mohammad, L., Mondal, I., 2024. Groundwater spring potential mapping:
1570 Assessment the contribution of hydrogeological factors. Advances in Space Research 74, 48–64.
1571 <https://doi.org/10.1016/j.asr.2024.03.038>.
- 1572
1573 Zheng, Y., Hu, Z., Wang, R., Wen, X., Ren, X., Pan, R., 2024. Slope Stability Analysis under Heavy Rainfall
1574 Conditions Based on a Modified Green-Ampt Model. Water Resour Manage 38, 2627–2646.
1575 <https://doi.org/10.1007/s11269-024-03790-3>.

Declaration of interests

- The authors declare that they have no known competing financial interests or personal relationships that could have appeared to influence the work reported in this paper.
- The author is an Editorial Board Member/Editor-in-Chief/Associate Editor/Guest Editor for *[Journal name]* and was not involved in the editorial review or the decision to publish this article.
- The authors declare the following financial interests/personal relationships which may be considered as potential competing interests:

